Amyloid β instigates cardiac neurotrophic signaling impairment, driving Alzheimer's associated heart disease

Andrea Elia[1], Rebecca Parodi-Rullan[1], Rafael Vazquez-Torres[1], Ashley Carey[1], Sabzali Javadov[2†], and Silvia Fossati[1].

[1]Alzheimer's Center at Temple (ACT), Department of Neural Sciences, Lewis Katz School of Medicine, Temple University, 3500 N Broad St, Philadelphia, PA 19140.

[2] Department of Physiology, University of Puerto Rico School of Medicine, San Juan, PR 00936-5067, USA

† Deceased.

Corresponding author: Silvia Fossati; silvia.fossati@temple.edu

Abstract

While a link between cardiovascular risk factors and increased Alzheimer's disease (AD) risk has been reported, it remains unclear whether AD pathology has a direct effect on cardiac function and myocardial innervation. AD and amyloidosis are known to impair neuronal function and affect brain neurotrophic factors (NGF and BDNF) expression. Amyloid aggregates and neuro-signaling impairments may also expose AD patients to peripheral nervous system deficits, promoting cardiac disorders. Here, we characterize cardiac physiology, amyloid pathology, neurotrophic factors loss, and the impoverishment of cardiac neuronal fibers in Tg2576-AD mice hearts, human cardiomyocytes in culture, and human AD post-mortem left ventricular (LV) heart tissue. We reveal that Tg2576 animals exhibit increased myocardial fibrosis, amyloid β (Aβ) deposition, and brain/heart-axis neurotrophic deficiencies, resulting in myocardial denervation and cardiac dysfunction. Aβ oligomers reduce BDNF expression in both human immortalized and iPSC-derived cardiomyocytes, by disrupting TrkB/CREB signaling. Analysis of human LV AD post-mortem tissue confirmed cell and animal results. Our findings elucidate a previously unknown mechanism of Aβ-induced cardiac neurotrophic signaling dysregulation, underscoring the relevance of heart degeneration in AD.

Keywords: Amyloid-β (Aβ); Alzheimer's disease; cardiac dysfunction; neuro-signaling pathway; iPSC-derived cardiomyocytes; human post-mortem heart; brain-heart axis

Translational Perspective

This research identified cardiac amyloid pathology, neurotrophic factor depletion, and reduced myocardial nerve function in a transgenic model of cerebral amyloidosis (Tg2576) and in human AD heart tissue. These findings carry significant diagnostic and therapeutic implications, emphasizing the role of neuro-signaling disruption in cardiac physiology impairment linked to AD. Our study advocates for considering cardiac complications in AD management and paves the way for future precision medicine approaches to enhance systemic clinical strategies for treating AD, proposing the cardiac neurotrophic signaling pathway as a potential therapeutic target.

1. Introduction

Alzheimer's disease (AD) is an escalating global health concern, anticipated to triplicate in prevalence by 2050, primarily due to population aging[1] . This complex neurodegenerative disorder is characterized by the progressive accumulation of insoluble amyloid-β (Aβ) plaques in the brain parenchyma together with neurofibrillary tangles formed by hyperphosphorylated tau. Besides Aβ plaques and tau buildups, about 90% of AD patients also show Aβ deposits in and around the cerebral vasculature, known as cerebral amyloid angiopathy (CAA). CAA contributes significantly to the progression of AD pathology by promoting neuroinflammation, neurovascular dysfunction, decreased brain clearance, increased blood-brain barrier (BBB) permeability, and eventually neurodegeneration[2,3].

Despite the main symptoms of the disease predominantly concerning the central nervous system (CNS), emerging evidence highlights extracerebral implications of AD, involving peripheral organs such as the heart[4]. Although abundant attention has been given to the impact of cardiovascular risk factors on AD risk and progression[5-7], only recent studies suggest a direct effect of AD pathology on cardiac dysfunction, and reveal Aβ peptides (Aβ40 and Aβ42) and big tau accumulation in the cardiac tissue of AD patients[8,9].

The accumulation of Aβ in the AD brain is known to significantly affect the expression of the two main neurotrophic factors, nerve growth factor (NGF) and brain-derived neurotrophic factor (BDNF) [10]. This neurosignaling pathway's maladaptive remodeling is associated with cognitive decline[11]. The production of neurotrophins such as BDNF is also important for peripheral organs and cells, including endothelial cells, muscle cells, and cardiomyocytes. BDNF operates through tropomyosin receptor kinase B (TrkB) stimulation, contributing to the activation of neuronal pro-survival genes, including BDNF itself, through cAMP response element-binding protein (CREB) signaling[12]. Additionally, BDNF exerts pleiotropic effects in endothelial cells, muscle cells, and cardiomyocytes. BDNF/TrkB/CREB signaling is crucial for proper heart development and function in adulthood[13]. It is plausible to hypothesize that the cerebral neurotrophic signaling degeneration in AD may be accompanied by a gradual decline also in peripheral levels and function of these neuromodulators. A lack of neurotrophic support may result in a severe derangement of the cardiac nervous system, potentially culminating in severe heart dysfunction. Notably, declining

circulating BDNF levels have also been linked to cardiac disease progression, particularly of ischemic origin[14].

However, the effects of AD pathology on the heart pathophysiology remain poorly understood, and whether and through what mechanisms AD and amyloidosis modulate NTFs levels and innervation in the cardiac tissue have not been previously explored. Also, whether specific Aβ aggregates such as toxic oligomers, which may accumulate in the AD heart, fuel cardiac neuro-signaling dysregulation, is still to be defined.

To address these questions, we analyzed whether and how the accumulation of cardiac Aβ aggregates affected peripheral innervation and NTFs expression in the heart of Tg2576 transgenic mice, one of the most widely used models of cerebral amyloidosis. We observed a progressive decline in cardiac function, that became significant in 13 months-old Tg mice compared to controls, and was accompanied by Aβ deposition, fibrosis, increase in cardiac mass and reduced contractility. We found a significant reduction in cardiac nerve fiber density and neurotrophins levels, adrenergic and neuronal fibers regeneration markers, in Tg2576 mice compared to controls. Through *in vitro* experiments on human AC16 cardiomyocytes, neuroblastoma cells, and validation in human-induced pluripotent Stem Cell-derived cardiomyocytes (hiPSC-CMs), we showed that exposure to Aβ oligomers significantly reduced the expression of BDNF in both neural and cardiac cells. BDNF acts through tropomyosin receptor kinase B (TrkB) stimulation, contributing to the activation of pro-survival genes, including BDNF itself, through cAMP response element-binding protein (CREB) signaling. We demonstrated that CREB levels were reduced in cardiomyocytes exposed to Aβ oligomers, and that a TrkB agonist could mitigate caspase 3 activation and apoptosis in Aβ-exposed cardiomyocytes. Finally, we validated these findings by analyzing the neurotrophic cardiac profile in human left ventricle (LV) post-mortem tissue from AD patients with CAA compared to age-matched heathy subjects, thus opening novel avenues for future investigations into the impact of AD pathology on cardiac physiology.

This study demonstrates that pathological Aβ oligomers induce cardiac neuro-signaling impairment in mouse models and human AD hearts, elucidates the molecular mechanism responsible for Aβ-mediated cardiac neurotrophic deficiency and nerve fiber loss in AD, and may suggest novel therapeutic avenues to tackle this devastating

disease, contributing to filling an important gap on the effects of AD on cardiac function and pathology.

2. Methods

Animal Model

Male and female Tg2576 mice, a model of cerebral amyloidosis bearing the Swedish mutation (KM670/671NL), and age-matched wild-type (WT) littermates were bred in-house. Mice were maintained under controlled conditions (~22°C and in a 12-hour light-dark cycle, lights from 7 am to 7 pm) with unrestricted access to food and water. The generation of B6; SJL-Tg (APPSWE)2576Kha mice (Tg2576) on a B6; SJL Mixed Background was described in[15] . Tg2576 mice are known to develop numerous cerebral parenchymal amyloid-β plaques at 11-13 months and CAA at 10-11 months[16]. All experiments and animal protocols were performed in equal numbers of male and female mice, according to procedures approved by the Institutional Animal Care and Use Committee of Temple University School of Medicine and conformed to the National Research Council Guide for the Care and Use of Laboratory Animals published by the US National Institutes of Health (2011, eighth edition).

Assessment of cardiac function by transthoracic echocardiography

Transthoracic bi-dimensional M-mode echocardiographic analysis was accomplished in 4, 8 and 13 months-old mice (before and after the development of brain Aβ pathology), under anesthesia, using a VisualSonics Vevo 2100 system (VisualSonics, Toronto, Canada). Before echocardiographic evaluation, the chest of the mice was carefully depilated by an operator. Subsequently, the mice were positioned in a clinostatic orientation on a temperature-controlled surface, with ECG leads embedded for monitoring, ensuring a constant temperature of 37°C. Anesthesia was then administered to the animals via an anesthetic chamber, utilizing isoflurane (Zoetis IsoFlo, Kalamazoo, MI), with an induction concentration of 3.0% and a maintenance range of 1–2.5%. This anesthesia regimen was meticulously managed to keep the animals within the desired anesthesia depth throughout the procedure, optimizing their physiological stability. Cardiac function and structure were evaluated by measuring left ventricle (LV) wall thickness, end-diastolic diameter (LVEDD), end-systolic diameter (LVESD), end-diastolic volume (LVEDV), end-systolic volume (LVESV), ejection fraction (EF%), and fraction shortening (FS%) percentage[17]. In accordance

141 with established protocols[18], speckle tracking-based strain echocardiography (STE)
142 was conducted using a parasternal long-axis B-mode loop captured through the
143 VisualSonics Vevo 2100 system (VisualSonics). High-speed imaging was ensured,
144 with all recordings comprising 300 frames at a rate exceeding 200 frames per second,
145 digitally stored as cine loops. Subsequently, the images obtained underwent
146 comprehensive analysis using Vevo Strain Software (Vevo LAB 1.7.1). LV endocardial
147 strain was computed in both radial and longitudinal axes and expressed as peak strain
148 percentage. Additionally, LV deformation rate over time was evaluated and presented
149 as strain rate (SR; peak 1/s). Global and regional assessments of LV endocardial
150 longitudinal and radial strain, along with SR, were performed based on the average
151 measurements derived from six LV segments (comprising basal, mid, and apical
152 anterior segments, as well as basal, mid, and apical posterior segments). Regional LV
153 endocardial longitudinal and radial strain, along with SR, were analyzed individually
154 for each LV segment and then averaged across both the anterior and posterior walls.
155 Vector diagrams illustrating the direction and magnitude of endocardial deformation
156 were acquired from parasternal long-axis B-mode images and subjected to detailed
157 analysis. Diastolic dysfunction was assessed by utilizing the reverse peak option to
158 evaluate reverse global longitudinal strain (GLS) and global radial strain (GRS) rates,
159 which were derived from long-axis B-mode traces[18,19]. Lastly, animals were
160 euthanized at 13 months for organ explant and biomolecular and histological analysis.

161 **Tissue processing and morphological evaluations**

162 Cardiac specimens were fixed in Zamboni's solution (2% paraformaldehyde and picric
163 acid) overnight at 4°C, then cryoprotected with 20% sucrose in PBS for 24 hours at
164 4°C and cut in 5-µm-consecutive thick longitudinal sections using a cryotome (Leica
165 2000R, Germany). Interstitial fibrosis was assessed via Picrosirius Red Stain Kit
166 (Abcam, ab150681), and images were acquired using a Nikon NiE Fluorescence
167 Microscope with an 20X objective[20]. Cardiac fibrosis density was measured using
168 ImageJ software (NIH, version 1.30) and expressed as a percentage of fibrotic area
169 over the total area. A single operator blindly executed all the quantifications.

170 **Immunostaining**

171 The cardiac sections were processed via the indirect immunofluorescence method
172 using rabbit polyclonal antibodies against tyrosine hydroxylase (TH, Millipore, AB152;

173 1:100) to stain adrenergic nerve fibers and growth association protein 43 (GAP-43,
174 Millipore, #AB5220; 1:100) for regenerating nerve terminals. Cardiac nerve fibers
175 showed a regular pattern along cardiomyocytes[21]. Heart nerve ending density was
176 quantified using a square grid with 24 probes (area: 1 cm^2 each) overlapped to the
177 digital images, which were acquired using a Nikon Eclipse Ti fluorescence microscope
178 with 20X and 60X objectives. Five areas were randomly chosen for quantification from
179 each sample's three sections. The total number of intercepts between nerve fibers and
180 probes for each area was assessed, and cardiac nerve fiber density was measured
181 and expressed as the mean number of intercepts per area (fibers/mm^2). A single
182 operator assessed all the measurements blindly. Next, to evaluate amyloid-β
183 accumulation, 5- μm-thick cardiac sections from each experimental group were
184 marked with 6E10 anti-Aβ antibody (Covance, SIG-39320; 1:500) and co-stained with
185 cardiac troponin T (cTnT, Thermo Scientific, #MA5-12960; 1:250), collagen type I
186 (Rockland Immunochemicals, #600-401-103-0.1; 1:100), cardiac Troponin I (cTnI,
187 Abcam, ab47003; 1:200), or cleaved caspase-3 (Asp175) (Cl-Casp-3, Cell Signaling,
188 #94530; 1:200) antibodies. Additionally, to characterize βsheet (fibrillar) amyloid
189 deposits, cardiac sections were stained with Thioflavin-S solution (Acros organics,
190 213150250; 0.5g of Thioflavin-S powder in 100 ml dH_2O) for 30 minutes at room
191 temperature shielding from the light. Next, the sections were dehydrated in 80%
192 ethanol and thus washed in PBS 1X buffer. Nuclei were labeled with 4', 6-diamidino-
193 2-phenylindole (DAPI, Sigma Aldrich, D9542; 1:5000), and sections were mounted
194 using an aqueous mounting medium. Digital images were captured and analyzed by
195 a Nikon Eclipse Ti fluorescence microscope with a 60X objective. To evaluate vascular
196 components, after fixation, cardiac specimens were cut into 5-μm-thick longitudinal
197 sections using a cryotome (Leica 2000R, Germany). Next, tissue sections were
198 incubated for 30' minutes at 4°C in a blocking solution (10% donkey serum
199 supplemented with 0.3% Triton X-100 in phosphate-buffered saline). Via indirect
200 immunofluorescence procedure, sections were analyzed using goat polyclonal
201 antibodies against CD31 (R&D Systems, AF3628-; 1:30) and α-smooth muscle actin
202 (α-SMA, Abcam, ab32575; 1:500) at 4°C overnight, followed by specific secondary
203 antibodies conjugated with cyanine 3 or cyanin 5 respectively, to stain vascular
204 network. For serum amyloid A3 immunostaining (SAA3), fixed 5-μm-thick cardiac
205 sections were retrieved with formic acid 70% solution (Thermo Scientific, #270480010)
206 for twenty minutes at room temperature, they were then stained using mouse

207 monoclonal antibody against SAA (Abbexa, abx018140, 1:50) for two hours at 37°C,
208 followed by specific secondary antibodies combined with Alexa Fluor 488-conjugated
209 anti-mouse IgG. DAPI was used to counterstain nuclei and cardiac sections were
210 mounted with a Vectashield vibrance antifade mounting medium (H-1000). To assess
211 the changes in the cross-sectional area (CSA) of cardiomyocytes, 5μm-thick cardiac
212 sections from each experimental group were incubated for 30 minutes at 4°C in a
213 blocking solution (10% donkey serum) and permeabilized with 0.3% Triton X-100 in
214 phosphate-buffered saline. The tissue sections were then stained with 5 μg/mL wheat
215 germ agglutinin (WGA, #W11261, Thermo Fisher Scientific, Waltham, MA, USA) as
216 previously described[22] (PMID: 34404991). Afterward, the sections were mounted with
217 Vectashield Vibrance antifade mounting medium (#H-1000). Digital images were
218 captured and analyzed using a Nikon Eclipse Ti fluorescence microscope with a 20X
219 objective. Five to six randomly selected fields per sample were analyzed, totaling 50-
220 60 cardiomyocytes per section (10 cells per area). The mean cardiomyocyte diameter
221 (μm) was measured using the ImageJ software. Lastly, to assess amyloid-β deposits
222 in the human heart, 5- μm-thick LV sections from healthy donors and AD with CAA
223 patients were stained with 6E10 anti-Aβ antibody (Covance, SIG-39320; 1:500) and
224 co-stained with cardiac Troponin I (cTnI, Abcam, ab47003; 1:200). Images were
225 acquired and examined using a Nikon Eclipse Ti fluorescence microscope with 20X
226 and 60X objectives. A single operator blindly performed all the procedures.

227 **Preparation of cell and tissue lysates and immunoblotting analysis**

228 Cellular and cardiac samples were homogenized using RIPA cell lysis buffer (Thermo
229 Scientific) enriched with phosphatases and protease inhibitors (Thermo Scientific).
230 Then, the lysates underwent sonication and were centrifuged for 10 minutes at 4°C at
231 13,000 rpm to discard the insoluble debris. Next, total protein amounts were quantified
232 via a dye-binding Pierce BCA protein assay kit (Thermo Scientific) and detected using
233 a spectrophotometer reader (SpectraMax i3x Multi-mode Microplate Reader,
234 Molecular Devices) at a wavelength of 562 nm. Equal yields of protein (20-40 μg) were
235 separated through SDS-PAGE and identified by western blot (WB) analysis. Total
236 lysates were used to evaluate the protein levels of NGF (Alomone labs, AN-240;
237 1:1000), BDNF (Alomone labs, ANT-010; 1:1000), GAP-43 (Millipore, #AB552;
238 1:1000), Cleaved Caspase-3- Asp175 (Cl-Casp-3, Cell Signaling, #94530; 1:500),
239 dopamine β hydroxylase (DβH, Millipore, #AB1536; 1:1000), human Aβ [mouse

240 monoclonal anti-Aβ antibodies mixture composed of 4G8 epitope (residues Aβ18-22,
241 Covance, SIG-39320; 1:1000) and 6E10 epitope (residues Aβ3-8, Covance, SIG-
242 39220; 1:1000)], serum amyloid A3 (SAA3, Abcam, #ab231680; 1:500) CREB (Cell
243 Signaling, #9197; 1:1000), fibronectin (Abcam, #ab2413; 1:1000), matrix
244 metalloproteinases- 2 (MMP-2, Cell Signaling, #35814; 1:1000), Laminin A/C (Santa
245 Cruz Biotechnology, sc-376248; 1:500), Actin (Millipore, MAB1501; 1:1000) and
246 GAPDH (Santa Cruz Biotechnology, sc-32233,6C5; 1: 2000), the three latter of which
247 were used as loading controls. Protein bands were detected using Odyssey® CLx
248 Imaging System according to the manufacturer's instructions and quantified with
249 Image Studio™ Lite Software[23].

250 **ELISA**

251 Aβ40 and Aβ42 peptide levels were detected using a commercial ELISA kit (Invitrogen
252 KHB3481 and KHB3441, respectively). Briefly, cardiac specimens for each mouse
253 were collected at the end of the experimental study and homogenized with RIPA cell
254 lysis buffer (Thermo Scientific), supplemented with phosphatases and protease
255 inhibitors (Thermo Scientific, Waltham, MA). Then, ELISA was performed using an
256 equal amount of total cardiac protein following the company's specifications, and the
257 plate was evaluated at 450 nm with a spectrophotometer reader (SpectraMax i3x
258 Multi-mode Microplate Reader, Molecular Devices).

259 **Aβ peptides**

260 Pre-aggregated Aβ40 and Aβ42 oligomers were generated from HFIP-pretreated and
261 lyophilized peptides as previously described[24]. Briefly, oligomer enriched Aβ40 and
262 Aβ42 preparations were obtained after a dilution of the lyophilized peptide in DMSO
263 at a concentration of 5 mM, then diluted to 100 μM in ice-cold DMEM/F12 media and
264 incubated at 4°C for 16 hours. Next, Aβ40 and Aβ42 oligomers were resuspended in
265 DMEM/F12 medium to 10 μM as a final concentration for the cell treatments.

266 **Cell culture and treatments**

267 Human ventricular myocardial cardiomyocytes (AC16, purchased from Millipore,
268 #SCC109) were expanded in 10 cm^2 dishes not further than the 10th passage, in a
269 humidified environment at 37°C with 5% CO_2 in DMEM/F12 medium (Lonza Ltd.
270 Basel, Switzerland) supplemented with 12.5% fetal bovine serum (FBS) and 1%

271 penicillin-streptomycin (P/S, Lonza). AC16 cells were grown in the pre-contractile
272 developmental stage, thus allowing us to better track molecular events and cellular
273 responses[25,26], without the complications and variability associated with isolated adult
274 cardiomyocyte cultures. Human SH-SY5Y neuroblastoma cells (ATCC, CRL-2266, a
275 neuronal cell line used widely in experimental neurological studies[27-29]) were grown in
276 10 cm^2 dishes within the 10th passage in a humidified environment at 37°C with 5%
277 CO_2 in DMEM/F12 medium (Lonza Ltd. Basel, Switzerland) supplemented with 10%
278 fetal bovine serum (FBS) and 1% penicillin-streptomycin (P/S, Lonza). For both cell
279 types, AC16 and SH-SY5Y, an equal number of cells were seeded in 6 well plates,
280 and after 24 hours, once they reached about 70- 80% confluency, cells were
281 challenged with human Aβ40 or Aβ42 oligomers (10 μM) for 16 hours. In certain
282 studies, cells were treated with human Aβ40 oligomers (10 μM) for either 15 minutes
283 or 1 hour. For other experiments, cells were exposed to the BDNF/TrkB receptor
284 agonist LM22A-4 (100 nM) or the antagonist ANA-12 (30 μM) for 16 hours. LM22A-4
285 (4607) and ANA-12 (SML0209) were sourced from Tocris Bioscience and Sigma
286 Aldrich, respectively.

287 **Maintenance and treatment of Human-Induced Pluripotent Stem Cell-Derived**
288 **Cardiomyocytes (hiPSC-CMs)**

289 A commercially available hiPSC-CM line, iCell Cardiomyocytes[2] (Catalog number
290 R1220, Kit/lot 12,012; FUJIFILM Irvine Scientific, Inc., United States), was utilized for
291 this study. The cells were seeded into a 0.1% gelatin-coated 12-well plate at a density
292 optimized to form a monolayer (≈210K cells per well) and cultured in a stage incubator
293 (37°C, 5% CO2) following the provider's guidelines. Experiments were conducted 5–
294 7 days post-plating, ensuring the cells formed a viable, beating monolayer, in
295 accordance with the manufacturer's instructions (Supplementary Video). Cells from
296 this specific lot were from the same donor (healthy, female, Caucasian, age <18), as
297 verified by FUJIFILM Cellular Dynamics. For the experiment, hiPSC-CMs were treated
298 with human Aβ40 oligomers (10 μM) for 20 hours, after which the cells were collected
299 for biochemical analysis. For imaging, cells were fixed with 4% paraformaldehyde
300 (PFA) for 10 minutes, washed with 1X PBS, and then blocked and permeabilized for
301 30 minutes using PBS containing 0.1% Triton X-100 and 2% normal donkey serum.
302 hiPSC-CMs were subsequently labeled with a BDNF antibody (Abcam, ab226843;
303 1:250) and co-stained for cardiac troponin T (cTnT, Thermo Scientific, #MA5-12960;

304 1:250), with nuclei labeled using DAPI (Sigma Aldrich, D9542; 1:5000). Imaging was
305 conducted using a Nikon Eclipse Ti fluorescence microscope with a 100X objective,
306 with all procedures performed by a single operator in a blinded manner.
307
308 **Nuclear protein isolation**
309 AC16 human cardiomyocytes were cultured in 6 well plates until they reached
310 confluence and treated with human Aβ40 oligomers for 15 minutes. To extract the
311 nuclear fractions, cells were collected using buffer A, containing 10 mmol/L HEPES at
312 pH 7.9, 10mmol/L KCl, 0.1mmol/L EDTA, integrated with 25% NP-40X-100 non-ionic
313 surfactant detergent solution, enriched with protease inhibitors. The cell lysate was
314 transferred in a 1.5 ml tube, placed in ice, and centrifuged for 10 min at 4°C at 13,000
315 rpm to discard the insoluble debris. The supernatant was transferred to a new 1.5 ml
316 tube to preserve the cytosolic fraction, while the pellet was resuspended in fresh
317 prepared buffer B composed of 20mmol/L HEPES at pH 7.9; 0.4mol/L NaCl; 1mmol/L
318 EDTA; 10% glycerol; supplemented with protease inhibitor. Next, the tube containing
319 the nuclei pellet dissolved in buffer B was placed on a rotator for 2 hours at 4°C and
320 then centrifuged at 13,000 rpm for 5 minutes at 4°C. Lastly, the supernatant (nuclear
321 fraction) was transferred to a new 1.5 ml tube and stored at -80°C, ready for the
322 following protein quantification and immunoblot analysis[23].
323
324 **Human LV specimens**
325 Frozen human LV post-mortem tissue from healthy donors and patients with clinical
326 diagnoses of AD and CAA were obtained from the Banner Sun Health Research
327 Institute clinical biobank to investigate the impact of AD pathology on myocardial
328 innervation. The selection criteria of the study population excluded individuals with
329 comorbidities known to substantially affect cardiac function, including high blood
330 pressure, cerebrovascular accidents (e.g., strokes and lacunes), brain/cardiac
331 neoplastic conditions, secondary amyloidosis, prior myocardial infarction, and
332 endocarditis. Healthy volunteers and AD+CAA patients were matched based on age,
333 sex, and ethnicity. Human cardiac specimens were used for biochemical and
334 histological characterization.
335
336
337

338 **Statistical methods and analysis**

339 Data are expressed as means±SEM. A two-tailed Student's t-test determined the
340 statistical significance between the two groups. When comparing multiple groups, data
341 were analyzed using a one-way or two-away analysis of variance (ANOVA) test,
342 followed by Tukey's post hoc test. Outliers were identified and excluded from the
343 original dataset using the ROUT (Q = 1%) method with GraphPad Prism 9.1.0
344 software. Differences between groups were considered statistically significant when
345 $p \leq 0.05$. All data were analyzed and graphically represented using GraphPad Prism
346 software version 9 (GraphPad, La Jolla, CA).

347 **3. Results**

348 **3.1. AD pathology promotes cardiac dysfunction, Aβ accumulation, and**
349 **misfolding of serum amyloid A3 in the heart of Tg2576 mice.**

350 To assess the impact of AD amyloid pathology on cardiac tissue physiology and
351 systolic activity, we conducted echocardiographic analyses in equal numbers of male
352 and female Tg2576 transgenic mice, and age-matched WT littermates, both before
353 and after the development of cerebral Aβ pathology (at 4 and 8, or 13 months,
354 respectively). Bi-dimensional M-mode tracings revealed a significant decrease in left
355 ventricular ejection fraction (EF%) and fractional shortening (FS%) percentage in 13-
356 month-old Tg2576 mice compared to WT animals (Fig. 1A-B, and other cardiac
357 echocardiographic parameters in Supplementary Table 1). Radial and longitudinal
358 strain/strain rates were also analyzed in both animal groups. Tg2576 exhibited global
359 (average of 6 LV segments) and anterior-apical longitudinal strain impairment
360 compared to WT mice, with severe longitudinal contractility dysfunction that affects the
361 anterior-basal segment (Supplementary Fig. 2). Younger Tg2576 cohorts (at 4 or 8
362 months) did not exhibit significant changes in cardiac physiology (Supplementary Fig.
363 3), despite the presence of Aβ deposits in the brain starting at 8 months
364 (Supplementary Fig. 5). Furthermore, 13-month-old transgenic mice displayed notable
365 left ventricle enlargement, evidenced by increased left ventricular end-systolic
366 diameter, leading to elevated left ventricular end-systolic volume (LVESV,
367 Supplementary Table 1). The gravimetric analysis confirmed a significant increase in
368 the heart weight/body weight ratio in 13-month-old Tg2576 mice compared to the WT
369 group (Fig. 1C), further corroborated by the increased cardiomyocyte cross-sectional

area assessed through WGA staining (Supplementary Fig. 1). Cardiac dysfunction in the Tg2576 mice coincided with a marked increase in myocardial interstitial fibrosis, as evidenced by Picrosirius red staining (Fig. 1D-E), accompanied by amyloid β accumulation in Tg2576 myocardial parenchyma (Fig. 1L) that contributes to a cardiac stiffness enhancement. Immunostaining results were confirmed via WB analysis, which shows high levels of fibronectin, a key component of the extracellular matrix (ECM) [30], in the Tg2576-AD mouse heart (Supplementary Fig. 1). However, in line with another recent AD study [31], no significant changes in cardiac MMP-2 levels between the WT and transgenic AD mice were observed (Supplementary Fig. 1).

Using peptide-specific ELISA assays, we confirmed a significant increase in Aβ40 levels in 13-month-old Tg2576 cardiac tissue compared to WT mice, while no substantial changes in Aβ42 levels were noted between the two groups (Fig. 1F-G). These findings align with the age dependent Aβ pathology in the Tg2576 mouse model, characterized by higher abundance and progressive increase in cerebral Aβ40 levels compared to Aβ42[32]. Western blot analysis further validated the cardiac Aβ40 deposition detected by ELISA, confirming a significant increase in Aβ dimers and oligomers in total heart lysates of 13 months old Tg2576 mice compared to WT littermates (Fig. 1H-I-J). Immunofluorescence staining revealed amyloid aggregates accumulating in interstitial spaces between cardiomyocytes, alongside collagen fibers, corroborating the myocardial interstitial fibrosis observed via Picrosirius red staining (Fig. 1L, top panels, and Supplementary Fig. 6B). Besides Aβ aggregates, reports have demonstrated amyloid precursor protein (APP) expression in peripheral organs, including the myocardium, suggesting the potential production of Aβ outside the brain parenchyma[9,33,34]. Consistent with this, but also with the fact that the prion protein promoter may be expressed in other innervated tissue, including in the heart, we observed APP upregulation in the plasma and cardiac tissue of Tg2576 mice (Supplementary Fig. 8). Aβ challenge has been linked to increased apoptosis in various cell types, including cardiac cells, and in AD brains[35,36]. Indeed, analysis of cardiac tissue by western blotting and immunohistochemistry revealed elevated levels of cleaved-caspase 3 in Tg2576 cardiomyocytes (Fig. 1K, 1L bottom panels, 1M).

As AD pathology is characterized by progressive protein misfolding, seeding processes may be initiated by different amyloids interacting with each other[37]. Therefore, the accumulation of misfolded Aβ oligomers in the heart tissue may contribute to increased fibrosis and to the seeding of other amyloid peptides, such as

404 serum amyloid A (SAA) proteins. Although high levels of SAAs typically do not lead to
405 fibrillar deposits, chronic inflammatory states or seeding processes (e.g., promoted by
406 Aβ) may induce the accumulation of SAA peptides in peripheral tissues[38,39]. Indeed,
407 we observed Aβ aggregates around cardiac vessels in aged Tg2576 mice,
408 accompanied by infiltration of the vascular basal lamina (Supplementary Fig. 4,
409 Supplementary Fig. 6, *bottom panels*, and Supplementary Fig. 7D), alongside
410 increased serum amyloid A3 (SAA3) vascular deposits (Fig. 1N). Immunoblot analysis
411 confirmed increased SAA3 dimers in the cardiac tissue of Tg2576 mice (Fig. 1O-P).
412 Overall, these findings indicate that AD pathology detrimentally affects systolic
413 function and cardiac tissue structure. Progressive interstitial and perivascular Aβ
414 deposits contribute to cardiac cell apoptosis and aggregation of serum amyloid
415 proteins, culminating in cardiovascular dysfunction. Notably, 8-month-old Tg2576
416 mice exhibited evident amyloid aggregate accumulation in the prefrontal cortex
417 vasculature and cerebral parenchyma (Supplementary Fig. 5), consistent with
418 literature describing early Aβ deposition and CAA in the Tg2576 brain[32]. However, no
419 significant changes were observed in Aβ accumulation in the hearts of 8-months old
420 Tg2576 mice compared to the older transgenic cohort (Supplementary Fig. 5 and
421 Supplementary Fig. 6), confirming that Aβ pathology starts in the brain of these mice,
422 followed by a later increase in cardiac Aβ levels.

423 **3.2. Neurotrophic signaling is impaired in the heart of AD transgenic mice.**

424 AD pathology and Aβ deposition are known to profoundly disrupt neurotrophins
425 production in the brain, contributing to the progressive loss of key neuromodulators,
426 including NGF and BDNF, ultimately leading to cognitive decline and dementia[40,41].
427 However, whether AD pathology can modulate peripheral neurotrophic activity and
428 cardiac innervation remained to be elucidated. Therefore, we explored the regulation
429 of neuro-signaling modulators and innervation factors in both cerebral cortex and
430 cardiac lysates of 13-month-old Tg2576 mice. Immunoblotting analysis revealed a
431 marked decrease in both cerebral and cardiac levels of NGF and BDNF expression in
432 the Tg2576 group compared to WT littermates (Fig. 2A-B). This reduction in
433 neurotrophins levels observed in transgenic mice was accompanied by a significant
434 decrease in the adrenergic marker (DβH) and the neuronal fibers regeneration marker,
435 GAP-43 (Fig. 2A-B). Intriguingly, immunohistochemistry analysis corroborated a
436 notable loss in cardiac nerve fiber density in Tg2576 mice compared to WT animals,

437 including reductions in sympathetic and regenerating nerve endings labeled with TH
438 and GAP-43 markers, respectively (Fig. 2C-D-E and Supplementary Fig. 7A-C). These
439 findings suggest that AD amyloid pathology may have detrimental effects on peripheral
440 neurotrophic pathways, thereby impacting the peripheral nervous system and cardiac
441 innervation.
442

443 **3.3. Aβ oligomers impair neurotrophins production in hiPSC-CMs, AC16**
444 **cardiomyocytes and neuroblastoma cells.**

445 Our *in vivo* investigations revealed a notable decrease in neurotrophic markers and
446 nerve fibers within the cardiac tissue of Tg2576 mice. To ascertain whether this loss
447 of NTFs can be caused by the Aβ aggregates present in the heart, we evaluated the
448 impact of Aβ40 oligomers, recognized as the most toxic amyloid aggregates and
449 preferentially enriched in the AD brain vasculature, on the production of neurotrophins
450 and neuronal regeneration markers in both human iPSC-CMs and AC16
451 cardiomyocytes (Fig. 3 and Fig. 4). Aβ40 oligomers significantly reduced BDNF
452 expression in hiPSC-CMs and AC16 cardiomyocytes (Fig. 3E-F and Fig. 4). In
453 addition, the effects of Aβ42 oligomers, the main toxic species coming in contact with
454 neurons in the brain parenchyma, were examined on neuronal SHSY-5Y cells.
455 Following a 16-hour incubation with Aβ oligomers, a significant reduction in protein
456 levels of GAP-43 and BDNF was observed in neuronal cells, with no substantial
457 changes in NGF expression (Fig. 3A-D). These findings support the hypothesis that
458 Aβ toxic aggregates contribute to the impairment of the cardiac neuro-signaling and
459 neural regeneration pathways by diminishing the production of BDNF in both neurons
460 and cardiomyocytes and reducing levels of GAP-43 in neurons.

461 **3.4. Neurotrophic factors are reduced in the heart of Alzheimer's disease**
462 **patients with cerebral amyloid angiopathy.**

463 To confirm the clinical and translational relevance of our findings in human AD, we
464 investigated the cardiac neurotrophic profile in LV biopsies obtained from patients
465 affected by AD along with CAA. Our study cohort comprised individuals clinically
466 diagnosed with AD, confirmed through anatomopathological examination, excluding
467 cases affected by other conditions that could significantly impair cardiac function, such
468 as high blood pressure, secondary amyloidosis, stroke, brain and cardiac neoplastic
469 conditions, prior myocardial infarction, and endocarditis. Healthy volunteers and

470 AD+CAA patients were matched based on age, sex, and ethnicity (Table 1). Our
471 analysis revealed significantly reduced levels of BDNF, downregulation of the
472 sympathetic marker tyrosine hydroxylase (TH), and a decline in GAP-43 protein
473 expression in the heart of AD+CAA subjects, confirming the deterioration of
474 neurotrophic factors and the neuro-signaling pathway in the human AD heart (Fig. 5A-
475 B), with enormous clinical implications. Immunostaining analysis showed amyloid-β
476 deposits in the myocardial parenchyma of human AD patients with CAA (Fig. 5C). In
477 aggregate, these findings demonstrate a myocardial neuro-signaling impairment
478 associated to Aβ deposition in human AD hearts, supporting our experimental *in vitro*
479 and *in vivo* results.

480 **3.5. Aβ40 oligomers impair BDNF/TrkB/CREB signaling in human**
481 **cardiomyocytes.**

482 The downregulation in BDNF expression observed in our *in vitro* and *in vivo*
483 experiments prompted us to investigate the mechanism by which Aβ affects the
484 cardiac BDNF pathway. BDNF/TrkB/CREB signaling impairment is involved in age-
485 related synaptic deterioration and neurodegenerative disorders, culminating in
486 cognitive decline and neuronal loss. Indeed, AD patients exhibit significant depletion
487 of BDNF expression in cerebrospinal fluid, post-mortem brain tissue, and
488 bloodstream[42]. The detrimental impact of Aβ oligomers on BDNF exon IV transcript in
489 neuronal cells is associated with decreased CREB levels, the critical mediator of
490 BDNF transcription[43,44]. Consistent with these findings, here we observed a significant
491 reduction in nuclear CREB levels in human cardiomyocytes following treatment with
492 Aβ40 oligomers (Fig. 6A-C), suggesting that a reduction in CREB transcriptional
493 function mediates both the reduced levels of BDNF and the impact on the other
494 neurotrophic markers. These results confirm the critical role of the BDNF/CREB axis
495 in AD cardiac pathology, unveiling an Aβ-dependent signaling mechanism which can
496 explain the BDNF reduction we observed in AD. To confirm the protective effect of
497 TrkB activation in our model, we stimulated human cardiomyocytes with the selective
498 TrkB receptor agonist, LM22A-4[45] (Fig. 6D-E), in the presence or absence of Aβ40
499 oligomers[46]. Remarkably, LM22A-4 stimulation reduced Aβ40-mediated caspase 3
500 activation, thereby mitigating apoptosis, and confirming the protective effects of BDNF
501 signaling on cardiac cells (Fig. 6G-H). Conversely, ANA-12, a specific BDNF/TrkB
502 receptor antagonist[47] (Fig. 6D-F), exacerbated cardiomyocyte caspase 3 activation,

503 (Fig. 6G-I), Overall, these findings elucidate the mechanisms and impact of the
504 neurotrophic signaling deregulation induced by Aβ pathology in the heart
505 (Supplementary Fig. 9), highlighting the protective role of BDNF/TrkB/CREB signaling
506 in cardiomyocyte homeostasis.

507 **4. Discussion**

508 This study demonstrates that, similar to what was previously observed in the brain, Aβ
509 deposition in the AD heart leads to neurotrophic signaling impairment, which
510 contributes to increased cardiomyocyte apoptosis and severe cardiac morphological
511 and functional impairment observed in the hearts of Tg2576 mice. Confirming the
512 clinical validity of these findings, the neurotrophic changes and the presence of Aβ
513 pathology were validated in human post-mortem heart samples from patients with
514 AD+CAA. Our data suggest that cardiac amyloidosis (evidenced by the presence of
515 Aβ and SAA3 oligomers) contributes to interstitial fibrosis and to the loss of
516 neurotrophins, resulting in cardiac innervation deficits and neuro-signaling pathway
517 impairment, which appear to be essential mediators of the observed cardiac
518 physiological dysfunction. The heart-brain axis constitutes a complex and highly
519 regulated bi-directional interconnection between the central and peripheral nervous
520 systems.[48]. Neurodegenerative pathologies, such as AD, may have severe and
521 debilitating effects on various peripheral organs, including the heart, through the
522 modulation of both the central and peripheral nervous systems. However, the impact
523 of AD pathology and Aβ accumulation on cardiac neuro-signaling pathways in AD
524 patients and animal models has not been previously elucidated. An increasing number
525 of studies are beginning to highlight the involvement of cardiac tissue in
526 neurodegenerative diseases, revealing a compelling interplay between AD and
527 cardiac disorders[49], such as atrial fibrillation[50], heart failure[51], and coronary artery
528 disease[34]. It has recently been shown that AD patients exhibit myocardial dysfunction
529 following the deposition of Aβ aggregates in cardiac tissue [9], and the presence of
530 cardiac N-terminal cleavage products of APP was correlated with levels of CAA and
531 myocardial fibrosis[52]. In line with this, Sanna and coworkers described the presence
532 of structural and functional abnormalities in the cardiac tissue of a small cohort of AD
533 subjects[4].
534 AD pathology has been shown to severely impact the production and release of the
535 main NTFs, NGF and BDNF, in the brain[53,54]. These two neurotrophins are mainly

536 involved in the maturation and differentiation of neurons, regulating neurogenesis and
537 synaptogenesis[55,56]. The progressive decline in NTFs expression due to aging,
538 exacerbated by AD pathology, may lead to an adverse remodeling of the whole neuro-
539 signaling pathway, driving, together with other AD pathological factors such as amyloid
540 oligomers, an impairment of the peripheral innervation[41].
541 This study demonstrates the effect of Aβ pathology on cardiac physiology and heart
542 dysfunction using a transgenic mouse model of AD with CAA, human cardiomyocytes
543 in culture, validated also in hiPSC-CMs, and AD+CAA human post-mortem heart
544 tissue. It describes the mechanisms underlying the impairment of peripheral
545 innervation and the loss of neurotrophins in the AD heart and shows a causal role of
546 Aβ oligomers in the impairment of neurotrophic signaling in cardiomyocytes. We report
547 that Tg2576 mice show an age-dependent deterioration in cardiac function and a
548 gradual replacement of viable myocardial with fibrotic tissue, resulting in interstitial
549 fibrosis. This cardiac maladaptive remodeling, which develops after the brain Aβ
550 deposition, is accompanied by an increased cross-sectional area alongside a
551 significant accumulation of Aβ, particularly Aβ40, localized in cardiac perivascular and
552 interstitial spaces with collagen deposits. Caspase 3 activation within cardiomyocytes
553 is also increased, suggesting that Aβ aggregates in the heart tissue contribute to the
554 development of interstitial fibrosis and apoptotic cardiac cell death. The preferential
555 accumulation of Aβ40, rather than Aβ42, in Tg2576 mice hearts is in line with previous
556 studies describing the progressive increase mostly of Aβ40 levels in both serum and
557 brain parenchyma of Tg2576 mice during aging[32]. Additionally, the Aβ40 peptide is
558 preferentially associated with vascular deposits and CAA in the human brain, resulting
559 in degenerative phenotypes in cerebral endothelial cells [36], which culminate in vessel
560 wall dysfunction[35], contributing to BBB permeability and microhemorrhages[57]. This
561 increased BBB permeability in AD brains may enhance the systemic diffusion of Aβ40
562 (including aggregated forms such as oligomers) through the blood and its
563 accumulation in peripheral organs, including the heart. Indeed, Aβ40 is the most
564 abundant peptide in the cerebrospinal fluid and blood of AD patients, and multiple
565 biomarker studies have shown that this peptide does not decrease in peripheral
566 organs and tissues with AD progression[58]. Conversely, as Aβ42 fibrils accumulate in
567 the brain parenchyma, Aβ42 levels decrease in the cerebrospinal fluid and in the
568 peripheral blood[59].

569 It is known that Aβ oligomers may act as “seeds”[60] to induce aggregation of other
570 amyloids. Some of these aggregation species fuel cell stress and inflammation,
571 resulting in degenerative processes in multiple cell types, including endothelial and
572 cardiac cells, as our group and others have shown[61,62]. Here, we show that SAA3 also
573 accumulates in the heart of Tg2576 mice, likely contributing to amorphous and
574 misfolded protein accumulation and to progressive cardiac impairment. SAA3 is
575 involved in vascular injury as a promoter of atherosclerosis, and it is a prognostic factor
576 for coronary artery syndromes, also proposed as a novel inflammatory marker for
577 ischemic heart disorders[63-65]. Notably, we observed SAA3 aggregates accumulate
578 primarily at the cardiac vessel walls, together with Aβ deposits, suggesting that
579 misfolded Aβ peptides or oligomers may diffuse through the vascular system, reaching
580 the heart, with consequential seeding of other systemic amyloids around the
581 myocardial vessels. Interestingly, no changes in cardiac physiology and no evidence
582 of amyloid deposits were found in younger (4 or 8 months) Tg2576 mice. However,
583 Aβ deposits were already detected around brain vessels in the prefrontal cortex of 8-
584 month-old Tg2576 mice. Thus, it is reasonable to think that, in this model and
585 presumably in AD patients, cardiac dysfunction may be subsequent to the progressive
586 accumulation of amyloid aggregates in the brain, particularly as CAA, in and around
587 the brain vessels. Given the extensive literature available on the vascular contributions
588 to cognitive impairment (VCID) field[5,66], we postulate that the cardiac disease and
589 maladaptive heart remodeling resulting from progressive amyloid deposition in the
590 heart also contribute to cognitive decline, thereby exacerbating AD pathology in a
591 destructive feed-forward loop.
592 Notably, we observed pro-apoptotic markers (active caspase 3) in cardiomyocytes
593 exposed to Aβ oligomers in vitro and in vivo, suggesting a direct effect of Aβ
594 pathological aggregates on the impairment of cardiac cell function. Interestingly,
595 caspase 3 activation is also associated with tau cleavage at position 421, which
596 promotes increased tau phosphorylation[67], suggesting possible downstream effects
597 that may precipitate tau pathology, which was recently described in the heart by the
598 Del Monte group[8,68]. Notably, we revealed a depletion in both adrenergic nerve
599 endings and regenerated nerve terminal fibers in the transgenic AD mouse hearts.
600 This myocardial denervation was associated with a reduction of NGF and BDNF at
601 both the cerebral and cardiac levels, accompanied by significant impairment in the
602 neuronal sprouting marker GAP-43. Importantly, post-mortem AD human hearts also

603 exhibited a reduction in BDNF expression, as well as in the cardiac nerve fiber markers
604 TH and GAP-43. In AD patients, the decline of neuromodulators in the brain is known
605 to accelerate age-related synaptic loss, resulting in cognitive impairment[69,70]. NTFs
606 are powerful biomolecules with significant pleiotropic effects involved in cellular growth
607 and survival pathways in both the brain and peripheral cells/tissues, including
608 endothelial cells, muscle cells, and the cardiovascular system[22]. Our finding that after
609 treatment with Aβ oligomers, BDNF and GAP-43 expression in human neurons,
610 endothelial cells, and both hiPSC-CMs-derived and immortalized cardiomyocytes
611 were significantly reduced suggests a direct effect of Aβ in lowering NTFs not only in
612 neuronal cells, and possibly peripheral neurons, but also in endothelial cells and
613 cardiomyocytes. This reduction may cause AD patients to be more susceptible to
614 developing cardiovascular disorders of various etiologies[71,72].
615
616 To validate the mechanism inducing this cardiac Aβ-mediated neuro-signaling
617 deterioration, we manipulated the BDNF signaling pathway pharmacologically in
618 human cardiomyocytes. Cells treated with LM22A-4, a competitive agonist of the
619 BDNF receptor TrkB, showed a reduction in Aβ40 oligomers-mediated caspase 3
620 activation, confirming a TrkB-dependent mechanism linking reduced BDNF to the Aβ-
621 mediated cardiomyocyte toxicity. LM22A-4 was also reported to alleviate cardiac
622 ischemia-induced apoptosis and to improve neuronal outgrowth and myocyte
623 physiology with endothelial cell proliferation, thus arresting chronic heart failure[14].
624 Moreover, LM22A-4 showed effects similar to BDNF in preventing Aβ-induced
625 neuronal cell death[45]. These beneficial effects suggest the initiation of a myocardial
626 autocrine/paracrine protective pathway through TrkB activation, which may include the
627 increased transcription of BDNF itself, via CREB activation[14].
628 In line with this concept, we demonstrated a significant downregulation of CREB
629 nuclear expression (necessary for its transcriptional function) in cardiomyocytes
630 challenged with Aβ40 oligomers. CREB is the leading transcription factor activated
631 upon BDNF-TrkB binding, which also promotes, in a feed-forward loop, the
632 transcription of BDNF itself. Our results provide a mechanistic explanation of how Aβ
633 oligomers can promote a CREB-mediated downregulation of BDNF expression in
634 cardiomyocytes, uncovering a previously unknown molecular pathway underlying the
635 AD-mediated cardiac neuro-signaling dysregulation. Notably, we demonstrated that
636 the cardiac tissue of AD patients with CAA exhibits significantly reduced neurotrophic

markers, including BDNF, together with Aβ deposits within the myocardial tissue. The presence of Aβ aggregates was also previously revealed in the human AD heart[9], reinforcing the relevance of our findings.

To our knowledge, this is the first study that investigated the impact of Aβ pathology on the neurotrophic signaling pathway in the AD heart and its effect on cardiovascular physiology in an AD animal model, with a validation of the loss of neurotrophic signaling mediators in human AD post-mortem cardiac tissue. These findings uncover a previously unrecognized dysfunction in the BDNF/TrkB/CREB signaling pathway, driven by Aβ accumulation within the cardiac nervous system. This disruption highlights neurotrophic signaling as a promising and novel pharmacological target for combating AD-induced cardiac dysfunction. While further clinical and translational studies are needed to fully validate these conclusions, our results strongly suggest that treating AD-related heart failure (HF) may require a therapeutic strategy specifically aimed at the cardiac neuronal system, that goes beyond conventional HF pharmacotherapy.

This emerging perspective calls for deeper investigation into the neuro-cardiac axis in AD. Importantly, our study opens a new translational avenue that may help personalize AD therapy in subjects with cardiac pathology, as well as characterize AD as a multi-organ neurodegenerative syndrome.

4.1 Limitations. While our study provides valuable insights into the cardiac implications of AD, several limitations should be acknowledged. First, we did not assess left ventricular diastolic function in our in vivo model, which has been implicated in previous studies of AD patients demonstrating diastolic impairment correlated with cardiac electrical abnormalities. Of note, given the advanced age of the animals used in the study, some technical difficulties do not always allow for consistent measurement of E/A ratios in all animals, given that the E and A waves overlap at a higher heart rate, as already demonstrated[18]. Therefore, the E/E′ ratio is not always considered a trustworthy measurement to assess the diastolic function in aging in vivo models, as also reported in murine heart failure with preserved ejection fraction and in volume overload models[19]. Accordingly, diastolic dysfunction was computed by using the reverse peak option to evaluate reverse global longitudinal strain (GLS) and global radial strain (GRS) rates, which were derived from long-axis B-mode traces. Moreover,

our focus on systolic function deterioration aligns with findings linking systolic impairment to cerebral hypoperfusion and emboli formation in AD patients, highlighting the connection between Aβ pathology and cardiovascular disease[73]. Additionally, due to the frailty of our AD mouse model and the desire to minimize stress-induced effects, we refrained from performing hemodynamic analysis, which could have provided further insights but may have impacted our animal population adversely[74]. Other neurotrophic factors, such as NT3 and NT4, may also contribute to cardiac innervation and function. Future investigations should explore the potential involvement of these factors in the AD myocardium to provide a comprehensive understanding of the cardiac neuro-signaling dysregulation. The potential of the BDNF/TrkB/CREB signaling reactivation to reverse or prevent cardiac dysfunction remains to be tested in vivo. Studies employing pharmacological strategies to increase cerebral amyloid clearance are also under development[75], to determine if reducing brain amyloid pathology may ameliorate heart function. Additionally, generating AD mouse models with BDNF cardiomyocyte-specific deletion could significantly enhance future research approaches. However, the combined mutations may lead to early morbidity and reduced lifespan[76,77], therefore careful experimental design and substantial investment in resources and technology will be needed. Furthermore, Aβ plaques exacerbate cellular stress and inflammation, driving degenerative processes across multiple cell types, including neurons and brain endothelial cells. This cascade worsens BBB breakdown and accelerates AD-induced maladaptive remodeling. In our study, we demonstrated that SAA3, a known inflammatory marker for ischemic heart disease[63-65], predominantly accumulates in the cardiac vessel walls of Tg2576-AD mice, together with Aβ deposits. This suggests that misfolded Aβ peptides or oligomers may infiltrate the vascular system, reaching the heart and fostering the seeding of other systemic amyloid deposition around myocardial vessels. These findings highlight the need for further investigation into the inflammatory dynamics of Alzheimer's heart pathology, an intriguing avenue for future research beyond the scope of this study. Lastly, the sample size of our human cardiac post-mortem specimens is limited, as obtaining human cardiac samples from AD patients without significant cardiovascular diseases is extremely challenging. Future, more comprehensive clinical studies are recommended to confirm AD cardiac dysfunction and validate the Aβ-mediated myocardial denervation observed in our study. Despite these limitations, our findings offer novel key insights into the pathophysiology of AD-

705 related cardiac dysfunction and underscore the need for further research to improve
706 the clinical management of AD patients.
707
708 **5. Conclusions.** In summary, our study elucidates a profound impact of AD amyloid
709 pathology on cardiac function, highlighting the maladaptive cardiac remodeling
710 characterized by amyloid deposition, fibrosis, and a previously unknown dysregulation
711 of the neurotrophic signaling pathway. The study also uncovers a mechanism whereby
712 Aβ-induced reduction in cardiac CREB activation impairs BDNF transcription,
713 ultimately leading to myocardial denervation, pro-apoptotic signaling, and cardiac
714 physiological dysfunction. These findings significantly contribute to our understanding
715 of AD pathophysiology, particularly Aβ-mediated cardiac dysfunction. Moreover, our
716 study identifies potential therapeutic targets within the neurotrophic signaling pathway
717 to mitigate the detrimental effects of AD and amyloid pathology on the cardiovascular
718 system, bridging the gap between molecular insights and potential for clinical
719 translation. Finally, this study underscores the importance of considering cardiac
720 complications in managing AD and offers promising avenues for future research and
721 therapeutic development.

722 **6. Acknowledgement**

723 We acknowledge that Supplementary Figure 9 was created using BioRender.com. We
724 thank the Brain and Body Donation Program Banner Sun Health Research Institute
725 clinical biobank for providing human LV post-mortem tissue. We thank Life Science
726 Editors for editing services.

727 **7. Funding**

728 This work was supported by NIH R01NS104127 and R01AG062572 grants, the
729 Alzheimer's Association (AARG-20-685663), and the Pennsylvania Department of
730 Health Collaborative Research on Alzheimer's Disease (PA Cure) Grant awarded to
731 SF, by the NIH SC1GM128210 grant awarded to SJ, by American Heart Association
732 Postdoctoral fellowship 24POST1240115 awarded to AE, by the Karen Toffler
733 Charitable Trust, and the Lemole Center for Integrated Lymphatics research.

734

8. Authors Contribution

AE and SF designed the study. AE performed and conceptualized the experiments and analyzed the data. AE wrote the paper draft and did the literature search. RPR, AC, and RVT performed experiments. SF provided relevant insights, scientific supervision, critically revised the manuscript and acquired funding. SJ revised the study, edited the manuscript, and offered additional literature searches.

9. Conflict of interest

The authors declare no conflicts of interest.

10. Data availability

The corresponding author will share the data underlying this article upon reasonable request.

11. References

1. Hebert LE, Weuve J, Scherr PA, Evans DA. Alzheimer disease in the United States (2010-2050) estimated using the 2010 census. *Neurology*. 2013;80:1778-1783. doi: 10.1212/WNL.0b013e31828726f5
2. Greenberg SM, Bacskai BJ, Hernandez-Guillamon M, Pruzin J, Sperling R, van Veluw SJ. Cerebral amyloid angiopathy and Alzheimer disease - one peptide, two pathways. *Nature reviews Neurology*. 2020;16:30-42. doi: 10.1038/s41582-019-0281-2
3. Masters CL, Bateman R, Blennow K, Rowe CC, Sperling RA, Cummings JL. Alzheimer's disease. *Nat Rev Dis Primers*. 2015;1:15056. doi: 10.1038/nrdp.2015.56
4. Sanna GD, Nusdeo G, Piras MR, Forteleoni A, Murru MR, Saba PS, Dore S, Sotgiu G, Parodi G, Ganau A. Cardiac Abnormalities in Alzheimer Disease: Clinical Relevance Beyond Pathophysiological Rationale and Instrumental Findings? *JACC Heart Fail*. 2019;7:121-128. doi: 10.1016/j.jchf.2018.10.022
5. Carey A, Fossati S. Hypertension and hyperhomocysteinemia as modifiable risk factors for Alzheimer's disease and dementia: New evidence, potential therapeutic strategies, and biomarkers. *Alzheimer's & dementia : the journal of the Alzheimer's Association*. 2023;19:671-695. doi: 10.1002/alz.12871
6. Hachinski V, Einhaupl K, Ganten D, Alladi S, Brayne C, Stephan BCM, Sweeney MD, Zlokovic B, Iturria-Medina Y, Iadecola C, et al. Preventing dementia by preventing stroke: The Berlin Manifesto. *Alzheimers Dement*. 2019;15:961-984. doi: 10.1016/j.jalz.2019.06.001
7. Saeed A, Lopez O, Cohen A, Reis SE. Cardiovascular Disease and Alzheimer's Disease: The Heart-Brain Axis. *J Am Heart Assoc*. 2023;12:e030780. doi: 10.1161/JAHA.123.030780
8. Luciani M, Montalbano M, Troncone L, Bacchin C, Uchida K, Daniele G, Jacobs Wolf B, Butler HM, Kiel J, Berto S, et al. Big tau aggregation disrupts microtubule tyrosination and causes myocardial diastolic dysfunction: from discovery to therapy. *Eur Heart J*. 2023;44:1560-1570. doi: 10.1093/eurheartj/ehad205
9. Troncone L, Luciani M, Coggins M, Wilker EH, Ho CY, Codispoti KE, Frosch MP, Kayed R, Del Monte F. Abeta Amyloid Pathology Affects the Hearts of Patients With Alzheimer's Disease: Mind the Heart. *J Am Coll Cardiol*. 2016;68:2395-2407. doi: 10.1016/j.jacc.2016.08.073

10. Allen SJ, Watson JJ, Dawbarn D. The neurotrophins and their role in Alzheimer's disease. *Curr Neuropharmacol*. 2011;9:559-573. doi: 10.2174/157015911798376190
11. Garzon D, Yu G, Fahnestock M. A new brain-derived neurotrophic factor transcript and decrease in brain-derived neurotrophic factor transcripts 1, 2 and 3 in Alzheimer's disease parietal cortex. *J Neurochem*. 2002;82:1058-1064. doi: 10.1046/j.1471-4159.2002.01030.x
12. Matthews VB, Astrom MB, Chan MH, Bruce CR, Krabbe KS, Prelovsek O, Akerstrom T, Yfanti C, Broholm C, Mortensen OH, et al. Brain-derived neurotrophic factor is produced by skeletal muscle cells in response to contraction and enhances fat oxidation via activation of AMP-activated protein kinase. *Diabetologia*. 2009;52:1409-1418. doi: 10.1007/s00125-009-1364-1
13. Kermani P, Hempstead B. BDNF Actions in the Cardiovascular System: Roles in Development, Adulthood and Response to Injury. *Front Physiol*. 2019;10:455. doi: 10.3389/fphys.2019.00455
14. Cannavo A, Jun S, Rengo G, Marzano F, Agrimi J, Liccardo D, Elia A, Keceli G, Altobelli GG, Marcucci L, et al. beta3AR-Dependent Brain-Derived Neurotrophic Factor (BDNF) Generation Limits Chronic Postischemic Heart Failure. *Circulation research*. 2023;132:867-881. doi: 10.1161/CIRCRESAHA.122.321583
15. Hsiao K, Chapman P, Nilsen S, Eckman C, Harigaya Y, Younkin S, Yang F, Cole G. Correlative memory deficits, Abeta elevation, and amyloid plaques in transgenic mice. *Science*. 1996;274:99-102. doi: 10.1126/science.274.5284.99
16. Robbins EM, Betensky RA, Domnitz SB, Purcell SM, Garcia-Alloza M, Greenberg C, Rebeck GW, Hyman BT, Greenberg SM, Frosch MP, et al. Kinetics of cerebral amyloid angiopathy progression in a transgenic mouse model of Alzheimer disease. *J Neurosci*. 2006;26:365-371. doi: 10.1523/JNEUROSCI.3854-05.2006
17. Rigaud VO, Zarka C, Kurian J, Harlamova D, Elia A, Kasatkin N, Johnson J, Behanan M, Kraus L, Pepper H, et al. UCP2 modulates cardiomyocyte cell cycle activity, acetyl-CoA, and histone acetylation in response to moderate hypoxia. *JCI Insight*. 2022;7. doi: 10.1172/jci.insight.155475
18. de Lucia C, Wallner M, Eaton DM, Zhao H, Houser SR, Koch WJ. Echocardiographic Strain Analysis for the Early Detection of Left Ventricular Systolic/Diastolic Dysfunction and Dyssynchrony in a Mouse Model of Physiological Aging. *J Gerontol A Biol Sci Med Sci*. 2019;74:455-461. doi: 10.1093/gerona/gly139
19. Schnelle M, Catibog N, Zhang M, Nabeebaccus AA, Anderson G, Richards DA, Sawyer G, Zhang X, Toischer K, Hasenfuss G, et al. Echocardiographic evaluation of diastolic function in mouse models of heart disease. *J Mol Cell Cardiol*. 2018;114:20-28. doi: 10.1016/j.yjmcc.2017.10.006
20. Cannavo A, Marzano F, Elia A, Liccardo D, Bencivenga L, Gambino G, Perna C, Rapacciuolo A, Cittadini A, Ferrara N, et al. Aldosterone Jeopardizes Myocardial Insulin and beta-Adrenergic Receptor Signaling via G Protein-Coupled Receptor Kinase 2. *Front Pharmacol*. 2019;10:888. doi: 10.3389/fphar.2019.00888
21. de Lucia C, Gambino G, Petraglia L, Elia A, Komici K, Femminella GD, D'Amico ML, Formisano R, Borghetti G, Liccardo D, et al. Long-Term Caloric Restriction Improves Cardiac Function, Remodeling, Adrenergic Responsiveness, and Sympathetic Innervation in a Model of Postischemic Heart Failure. *Circ Heart Fail*. 2018;11:e004153. doi: 10.1161/CIRCHEARTFAILURE.117.004153
22. Elia A, Cannavo A, Gambino G, Cimini M, Ferrara N, Kishore R, Paolocci N, Rengo G. Aging is associated with cardiac autonomic nerve fiber depletion and reduced cardiac and circulating BDNF levels. *J Geriatr Cardiol*. 2021;18:549-559. doi: 10.11909/j.issn.1671-5411.2021.07.009
23. Marzano F, Liccardo D, Elia A, Mucio I, de Lucia C, Lucchese AM, Gao E, Ferrara N, Rapacciuolo A, Paolocci N, et al. Genetic Catalytic Inactivation of GRK5 Impairs Cardiac Function in Mice Via Dysregulated P53 Levels. *JACC Basic Transl Sci*. 2022;7:366-380. doi: 10.1016/j.jacbts.2022.01.001

24. Fossati S, Giannoni P, Solesio ME, Cocklin SL, Cabrera E, Ghiso J, Rostagno A. The carbonic anhydrase inhibitor methazolamide prevents amyloid beta-induced mitochondrial dysfunction and caspase activation protecting neuronal and glial cells in vitro and in the mouse brain. *Neurobiol Dis*. 2016;86:29-40. doi: 10.1016/j.nbd.2015.11.006
25. Davidson MM, Nesti C, Palenzuela L, Walker WF, Hernandez E, Protas L, Hirano M, Isaac ND. Novel cell lines derived from adult human ventricular cardiomyocytes. *J Mol Cell Cardiol*. 2005;39:133-147. doi: 10.1016/j.yjmcc.2005.03.003
26. Lippi M, Stadiotti I, Pompilio G, Sommariva E. Human Cell Modeling for Cardiovascular Diseases. *Int J Mol Sci*. 2020;21. doi: 10.3390/ijms21176388
27. Grimm MOW, Blumel T, Lauer AA, Janitschke D, Stahlmann C, Mett J, Haupenthal VJ, Miederer AM, Niemeyer BA, Grimm HS, et al. The impact of capsaicinoids on APP processing in Alzheimer's disease in SH-SY5Y cells. *Sci Rep*. 2020;10:9164. doi: 10.1038/s41598-020-66009-6
28. Koriyama Y, Furukawa A, Muramatsu M, Takino J, Takeuchi M. Glyceraldehyde caused Alzheimer's disease-like alterations in diagnostic marker levels in SH-SY5Y human neuroblastoma cells. *Sci Rep*. 2015;5:13313. doi: 10.1038/srep13313
29. Riegerova P, Brejcha J, Bezdekova D, Chum T, Masinova E, Cermakova N, Ovsepian SV, Cebecauer M, Stefl M. Expression and Localization of AbetaPP in SH-SY5Y Cells Depends on Differentiation State. *J Alzheimers Dis*. 2021;82:485-491. doi: 10.3233/JAD-201409
30. Schwarzbauer JE, DeSimone DW. Fibronectins, their fibrillogenesis, and in vivo functions. *Cold Spring Harb Perspect Biol*. 2011;3. doi: 10.1101/cshperspect.a005041
31. Aishwarya R, Abdullah CS, Remex NS, Bhuiyan MAN, Lu XH, Dhanesha N, Stokes KY, Orr AW, Kevil CG, Bhuiyan MS. Diastolic dysfunction in Alzheimer's disease model mice is associated with Abeta-amyloid aggregate formation and mitochondrial dysfunction. *Sci Rep*. 2024;14:16715. doi: 10.1038/s41598-024-67638-x
32. Kawarabayashi T, Younkin LH, Saido TC, Shoji M, Ashe KH, Younkin SG. Age-dependent changes in brain, CSF, and plasma amyloid (beta) protein in the Tg2576 transgenic mouse model of Alzheimer's disease. *J Neurosci*. 2001;21:372-381. doi: 10.1523/JNEUROSCI.21-02-00372.2001
33. Kuo YM, Kokjohn TA, Watson MD, Woods AS, Cotter RJ, Sue LI, Kalback WM, Emmerling MR, Beach TG, Roher AE. Elevated abeta42 in skeletal muscle of Alzheimer disease patients suggests peripheral alterations of AbetaPP metabolism. *Am J Pathol*. 2000;156:797-805. doi: 10.1016/s0002-9440(10)64947-4
34. Tublin JM, Adelstein JM, Del Monte F, Combs CK, Wold LE. Getting to the Heart of Alzheimer Disease. *Circ Res*. 2019;124:142-149. doi: 10.1161/CIRCRESAHA.118.313563
35. Fossati S, Ghiso J, Rostagno A. TRAIL death receptors DR4 and DR5 mediate cerebral microvascular endothelial cell apoptosis induced by oligomeric Alzheimer's Abeta. *Cell Death Dis*. 2012;3:e321. doi: 10.1038/cddis.2012.55
36. Parodi-Rullan R, Ghiso J, Cabrera E, Rostagno A, Fossati S. Alzheimer's amyloid beta heterogeneous species differentially affect brain endothelial cell viability, blood-brain barrier integrity, and angiogenesis. *Aging Cell*. 2020;19:e13258. doi: 10.1111/acel.13258
37. Dobson CM. Principles of protein folding, misfolding and aggregation. *Semin Cell Dev Biol*. 2004;15:3-16. doi: 10.1016/j.semcdb.2003.12.008
38. De Buck M, Gouwy M, Wang JM, Van Snick J, Opdenakker G, Struyf S, Van Damme J. Structure and Expression of Different Serum Amyloid A (SAA) Variants and their Concentration-Dependent Functions During Host Insults. *Curr Med Chem*. 2016;23:1725-1755. doi: 10.2174/0929867323666160418114600
39. den Hartigh LJ, May KS, Zhang XS, Chait A, Blaser MJ. Serum amyloid A and metabolic disease: evidence for a critical role in chronic inflammatory conditions. *Front Cardiovasc Med*. 2023;10:1197432. doi: 10.3389/fcvm.2023.1197432

878 40. Arancio O, Chao MV. Neurotrophins, synaptic plasticity and dementia. *Curr Opin Neurobiol*.
879 2007;17:325-330. doi: 10.1016/j.conb.2007.03.013
880 41. Nasrolahi A, Javaherforooshzadeh F, Jafarzadeh-Gharehziaaddin M, Mahmoudi J, Asl KD,
881 Shabani Z. Therapeutic potential of neurotrophic factors in Alzheimer's Disease. *Mol Biol Rep*.
882 2022;49:2345-2357. doi: 10.1007/s11033-021-06968-9
883 42. Du Y, Wu HT, Qin XY, Cao C, Liu Y, Cao ZZ, Cheng Y. Postmortem Brain, Cerebrospinal Fluid,
884 and Blood Neurotrophic Factor Levels in Alzheimer's Disease: A Systematic Review and Meta-
885 Analysis. *J Mol Neurosci*. 2018;65:289-300. doi: 10.1007/s12031-018-1100-8
886 43. Esvald EE, Tuvikene J, Sirp A, Patil S, Bramham CR, Timmusk T. CREB Family Transcription
887 Factors Are Major Mediators of BDNF Transcriptional Autoregulation in Cortical Neurons. *J*
888 *Neurosci*. 2020;40:1405-1426. doi: 10.1523/JNEUROSCI.0367-19.2019
889 44. Garzon DJ, Fahnestock M. Oligomeric amyloid decreases basal levels of brain-derived
890 neurotrophic factor (BDNF) mRNA via specific downregulation of BDNF transcripts IV and V in
891 differentiated human neuroblastoma cells. *J Neurosci*. 2007;27:2628-2635. doi:
892 10.1523/JNEUROSCI.5053-06.2007
893 45. Massa SM, Yang T, Xie Y, Shi J, Bilgen M, Joyce JN, Nehama D, Rajadas J, Longo FM. Small
894 molecule BDNF mimetics activate TrkB signaling and prevent neuronal degeneration in
895 rodents. *J Clin Invest*. 2010;120:1774-1785. doi: 10.1172/JCI41356
896 46. Anzovino A, Canepa E, Alves M, Lemon NL, Carare RO, Fossati S. Amyloid Beta Oligomers
897 Activate Death Receptors and Mitochondria-Mediated Apoptotic Pathways in Cerebral
898 Vascular Smooth Muscle Cells; Protective Effects of Carbonic Anhydrase Inhibitors. *Cells*.
899 2023;12. doi: 10.3390/cells12242840
900 47. Cazorla M, Premont J, Mann A, Girard N, Kellendonk C, Rognan D. Identification of a low-
901 molecular weight TrkB antagonist with anxiolytic and antidepressant activity in mice. *J Clin*
902 *Invest*. 2011;121:1846-1857. doi: 10.1172/JCI43992
903 48. Tahsili-Fahadan P, Geocadin RG. Heart-Brain Axis: Effects of Neurologic Injury on
904 Cardiovascular Function. *Circ Res*. 2017;120:559-572. doi: 10.1161/CIRCRESAHA.116.308446
905 49. Elia A, Fossati S. Autonomic nervous system and cardiac neuro-signaling pathway modulation
906 in cardiovascular disorders and Alzheimer's disease. *Front Physiol*. 2023;14:1060666. doi:
907 10.3389/fphys.2023.1060666
908 50. Ihara M, Washida K. Linking Atrial Fibrillation with Alzheimer's Disease: Epidemiological,
909 Pathological, and Mechanistic Evidence. *J Alzheimers Dis*. 2018;62:61-72. doi: 10.3233/JAD-
910 170970
911 51. Cermakova P, Eriksdotter M, Lund LH, Winblad B, Religa P, Religa D. Heart failure and
912 Alzheimer's disease. *J Intern Med*. 2015;277:406-425. doi: 10.1111/joim.12287
913 52. Kramer LM, Brettschneider J, Lennerz JK, Walcher D, Fang L, Rosenbohm A, Balakrishnan K,
914 Benckendorff J, Moller P, Just S, et al. Amyloid precursor protein-fragments-containing
915 inclusions in cardiomyocytes with basophilic degeneration and its association with cerebral
916 amyloid angiopathy and myocardial fibrosis. *Sci Rep*. 2018;8:16594. doi: 10.1038/s41598-018-
917 34808-7
918 53. Cade S, Zhou XF, Bobrovskaya L. The role of brain-derived neurotrophic factor and the
919 neurotrophin receptor p75NTR in age-related brain atrophy and the transition to Alzheimer's
920 disease. *Rev Neurosci*. 2022;33:515-529. doi: 10.1515/revneuro-2021-0111
921 54. Gao L, Zhang Y, Sterling K, Song W. Brain-derived neurotrophic factor in Alzheimer's disease
922 and its pharmaceutical potential. *Transl Neurodegener*. 2022;11:4. doi: 10.1186/s40035-022-
923 00279-0
924 55. Vitaliano GD, Kim JK, Kaufman MJ, Adam CW, Zeballos G, Shanmugavadivu A, Subburaju S,
925 McLaughlin JP, Lukas SE, Vitaliano F. Clathrin-nanoparticles deliver BDNF to hippocampus and
926 enhance neurogenesis, synaptogenesis and cognition in HIV/neuroAIDS mouse model.
927 *Commun Biol*. 2022;5:236. doi: 10.1038/s42003-022-03177-3

928 56. Wang CS, Kavalali ET, Monteggia LM. BDNF signaling in context: From synaptic regulation to
929 psychiatric disorders. *Cell*. 2022;185:62-76. doi: 10.1016/j.cell.2021.12.003
930 57. Ghiso J, Fossati S, Rostagno A. Amyloidosis associated with cerebral amyloid angiopathy: cell
931 signaling pathways elicited in cerebral endothelial cells. *J Alzheimers Dis*. 2014;42 Suppl
932 3:S167-176. doi: 10.3233/JAD-140027
933 58. Hanon O, Vidal JS, Lehmann S, Bombois S, Allinquant B, Baret-Rose C, Treluyer JM, Abdoul H,
934 Gele P, Delmaire C, et al. Plasma amyloid beta predicts conversion to dementia in subjects
935 with mild cognitive impairment: The BALTAZAR study. *Alzheimers Dement*. 2022;18:2537-
936 2550. doi: 10.1002/alz.12613
937 59. Zicha S, Bateman RJ, Shaw LM, Zetterberg H, Bannon AW, Horton WA, Baratta M, Kolb HC,
938 Dobler I, Mordashova Y, et al. Comparative analytical performance of multiple plasma
939 Abeta42 and Abeta40 assays and their ability to predict positron emission tomography
940 amyloid positivity. *Alzheimers Dement*. 2023;19:956-966. doi: 10.1002/alz.12697
941 60. Ulm BS, Borchelt DR, Moore BD. Remodeling Alzheimer-amyloidosis models by seeding. *Mol*
942 *Neurodegener*. 2021;16:8. doi: 10.1186/s13024-021-00429-4
943 61. Jang S, Chapa-Dubocq XR, Parodi-Rullan RM, Fossati S, Javadov S. Beta-Amyloid Instigates
944 Dysfunction of Mitochondria in Cardiac Cells. *Cells*. 2022;11. doi: 10.3390/cells11030373
945 62. Parodi-Rullan RM, Javadov S, Fossati S. Dissecting the Crosstalk between Endothelial
946 Mitochondrial Damage, Vascular Inflammation, and Neurodegeneration in Cerebral Amyloid
947 Angiopathy and Alzheimer's Disease. *Cells*. 2021;10. doi: 10.3390/cells10112903
948 63. Chait A, Wang S, Goodspeed L, Gomes D, Turk KE, Wietecha T, Tang J, Storey C, O'Brien KD,
949 Rubinow KB, et al. Sexually Dimorphic Relationships Among Saa3 (Serum Amyloid A3),
950 Inflammation, and Cholesterol Metabolism Modulate Atherosclerosis in Mice. *Arterioscler*
951 *Thromb Vasc Biol*. 2021;41:e299-e313. doi: 10.1161/ATVBAHA.121.316066
952 64. Johnson BD, Kip KE, Marroquin OC, Ridker PM, Kelsey SF, Shaw LJ, Pepine CJ, Sharaf B, Bairey
953 Merz CN, Sopko G, et al. Serum amyloid A as a predictor of coronary artery disease and
954 cardiovascular outcome in women: the National Heart, Lung, and Blood Institute-Sponsored
955 Women's Ischemia Syndrome Evaluation (WISE). *Circulation*. 2004;109:726-732. doi:
956 10.1161/01.CIR.0000115516.54550.B1
957 65. Morrow DA, Rifai N, Antman EM, Weiner DL, McCabe CH, Cannon CP, Braunwald E. Serum
958 amyloid A predicts early mortality in acute coronary syndromes: A TIMI 11A substudy. *J Am*
959 *Coll Cardiol*. 2000;35:358-362. doi: 10.1016/s0735-1097(99)00574-4
960 66. Corriveau RA, Bosetti F, Emr M, Gladman JT, Koenig JI, Moy CS, Pahigiannis K, Waddy SP,
961 Koroshetz W. The Science of Vascular Contributions to Cognitive Impairment and Dementia
962 (VCID): A Framework for Advancing Research Priorities in the Cerebrovascular Biology of
963 Cognitive Decline. *Cell Mol Neurobiol*. 2016;36:281-288. doi: 10.1007/s10571-016-0334-7
964 67. Rissman RA, Poon WW, Blurton-Jones M, Oddo S, Torp R, Vitek MP, LaFerla FM, Rohn TT,
965 Cotman CW. Caspase-cleavage of tau is an early event in Alzheimer disease tangle pathology.
966 *J Clin Invest*. 2004;114:121-130. doi: 10.1172/JCI20640
967 68. Conze C, Rierola M, Trushina NI, Peters M, Janning D, Holzer M, Heinisch JJ, Arendt T, Bakota
968 L, Brandt R. Caspase-cleaved tau is senescence-associated and induces a toxic gain of function
969 by putting a brake on axonal transport. *Mol Psychiatry*. 2022;27:3010-3023. doi:
970 10.1038/s41380-022-01538-2
971 69. Hoth KF, Poppas A, Moser DJ, Paul RH, Cohen RA. Cardiac dysfunction and cognition in older
972 adults with heart failure. *Cogn Behav Neurol*. 2008;21:65-72. doi:
973 10.1097/WNN.0b013e3181799dc8
974 70. Numakawa T, Odaka H. The Role of Neurotrophin Signaling in Age-Related Cognitive Decline
975 and Cognitive Diseases. *Int J Mol Sci*. 2022;23. doi: 10.3390/ijms23147726
976 71. Bahls M, Konemann S, Markus MRP, Wenzel K, Friedrich N, Nauck M, Volzke H, Steveling A,
977 Janowitz D, Grabe HJ, et al. Brain-derived neurotrophic factor is related with adverse cardiac
978 remodeling and high NTproBNP. *Sci Rep*. 2019;9:15421. doi: 10.1038/s41598-019-51776-8

979 72. Takashio S, Sugiyama S, Yamamuro M, Takahama H, Hayashi T, Sugano Y, Izumiya Y, Hokimoto
980 S, Minamino N, Yasuda S, et al. Significance of low plasma levels of brain-derived neurotrophic
981 factor in patients with heart failure. *Am J Cardiol*. 2015;116:243-249. doi:
982 10.1016/j.amjcard.2015.04.018
983 73. Tini G, Scagliola R, Monacelli F, La Malfa G, Porto I, Brunelli C, Rosa GM. Alzheimer's Disease
984 and Cardiovascular Disease: A Particular Association. *Cardiol Res Pract*. 2020;2020:2617970.
985 doi: 10.1155/2020/2617970
986 74. Miranda-Silva D, Sequeira V, Lourenco AP, Falcao-Pires I. Assessing Rodent Cardiac Function
987 in vivo Using Hemodynamic Pressure-Volume Loops. *Front Physiol*. 2021;12:751326. doi:
988 10.3389/fphys.2021.751326
989 75. Canepa E, Parodi-Rullan R, Vazquez-Torres R, Gamallo-Lana B, Guzman-Hernandez R, Lemon
990 NL, Angiulli F, Debure L, Ilies MA, Ostergaard L, et al. FDA-approved carbonic anhydrase
991 inhibitors reduce amyloid beta pathology and improve cognition, by ameliorating
992 cerebrovascular health and glial fitness. *Alzheimers Dement*. 2023;19:5048-5073. doi:
993 10.1002/alz.13063
994 76. Jankowsky JL, Zheng H. Practical considerations for choosing a mouse model of Alzheimer's
995 disease. *Mol Neurodegener*. 2017;12:89. doi: 10.1186/s13024-017-0231-7
996 77. Zhong MZ, Peng T, Duarte ML, Wang M, Cai D. Updates on mouse models of Alzheimer's
997 disease. *Mol Neurodegener*. 2024;19:23. doi: 10.1186/s13024-024-00712-0

998

Figures

Figure 1

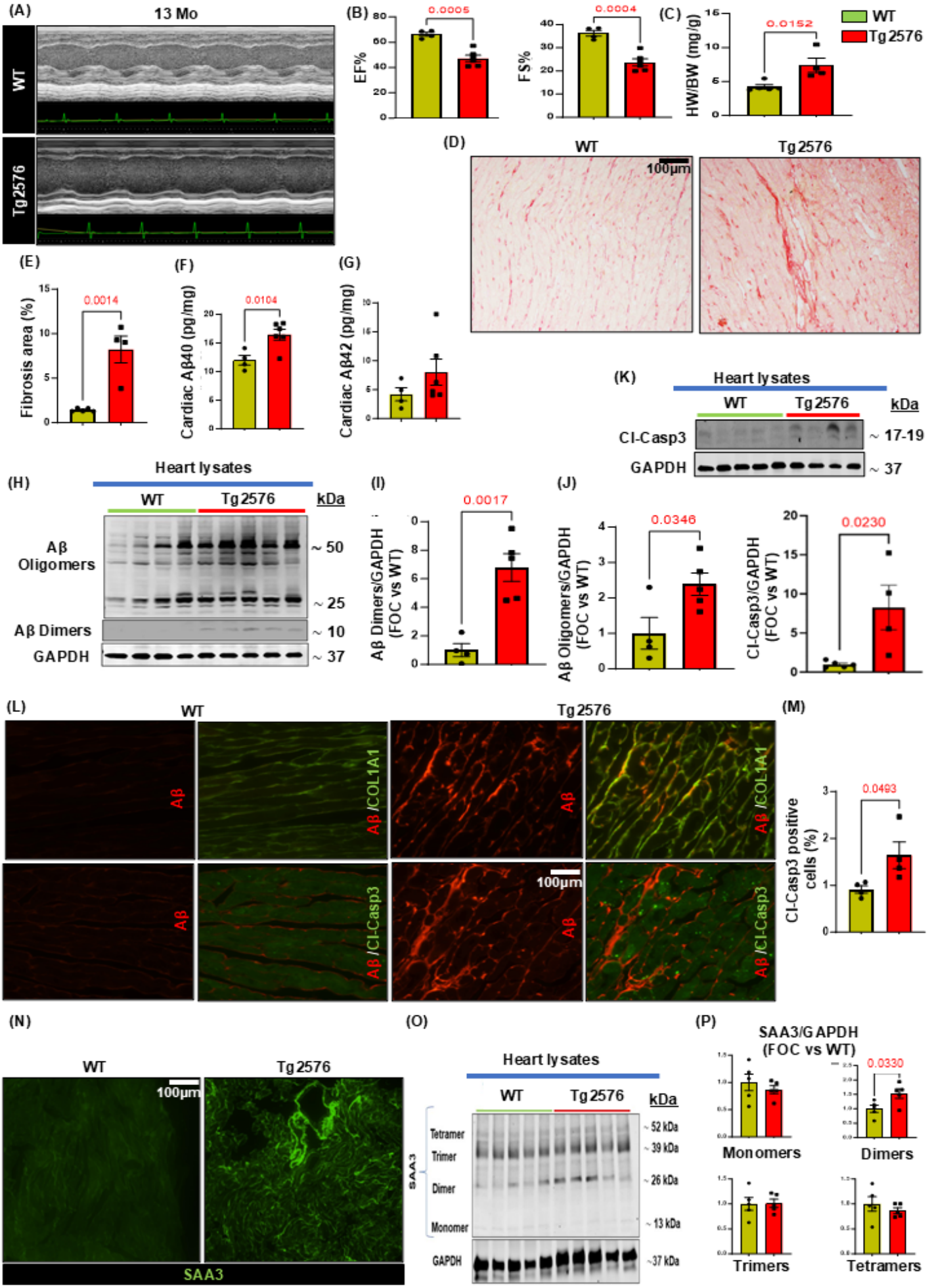

1000 **Figure 1. Cardiac physiological impairment, myocardial Aβ aggregates**
1001 **accumulation, cardiac cell apoptosis and Serum amyloid A3 (SAA3) deposition**
1002 **in the heart of Tg2576 AD mice.** (**A**) M-mode representative images of
1003 echocardiographic analysis in 13-month-old WT and Tg2576 mice. (**B**) Left ventricle
1004 (LV) function is impaired in the AD model, as evidenced by a significant decline both
1005 in ejection fraction (EF%) and fraction shortening percentage (FS%) showed by the
1006 Tg2576 group compared to WT mice age-matched (13-months-old). (**C**) The heart
1007 weight/body weight ratio is significantly increased in Tg2576 mice compared to the WT
1008 group. (**D**-**E**) Representative images (left panels) and quantitative data (right panels)
1009 showing the percentage (%) of fibrotic area in cardiac sections from WT and Tg2576
1010 mice, assessed via Picrosirius red staining (scale bar 50μm). (**F**-**G**): Aβ40 (**F**) Aβ42
1011 (**G**) cardiac levels (pg/mg of proteins), assessed by ELISA assay, in total cardiac
1012 lysates from WT and Tg2576 mice. (**H**-**J**): Representative immunoblots (left panels)
1013 and densitometric quantitative analysis (right panels) showing protein levels of Aβ
1014 dimers, oligomers (**I**-**J**) in total cardiac lysates from WT and Tg2576 mice. GAPDH
1015 levels were used as a loading control. (**K**): Representative immunoblots (upper panels)
1016 and densitometric quantitative analysis (lower panels) showing protein levels of
1017 Cleaved-Caspase3 (Cl-Casp3) in total cardiac lysates from WT and Tg2576 mice.
1018 GAPDH levels were used as a loading control. (**L**): Representative digital images
1019 (upper panels, scale bar 100μm) showing collagen type I fibers (COL1A1, in green)
1020 and Aβ (in red) and representative digital images (lower panels; scale bar 100μm) and
1021 quantification (**M**) showing Cleaved-Caspase3 (Cl-Casp3, in green) and Aβ (in red) in
1022 cardiac sections from WT and Tg2576 mice. (**N**): Representative WT and Tg2576
1023 cardiac sections stained for serum amyloid A3 (SAA3, in green, scale bar 100μm). (**O**-
1024 **P**): Representative immunoblots (**O**) and densitometric quantitative analysis (**P**)
1025 showing levels of different aggregates of SAA3 in total cardiac lysates from WT and
1026 Tg2576 mice. GAPDH levels were used as a loading control. n=4-6 mice/group. Data
1027 are presented as a mean±SEM. *P<0.05 and vs WT. Student t-tests were performed
1028 between the groups.

1029

1030

1031

Figure 2

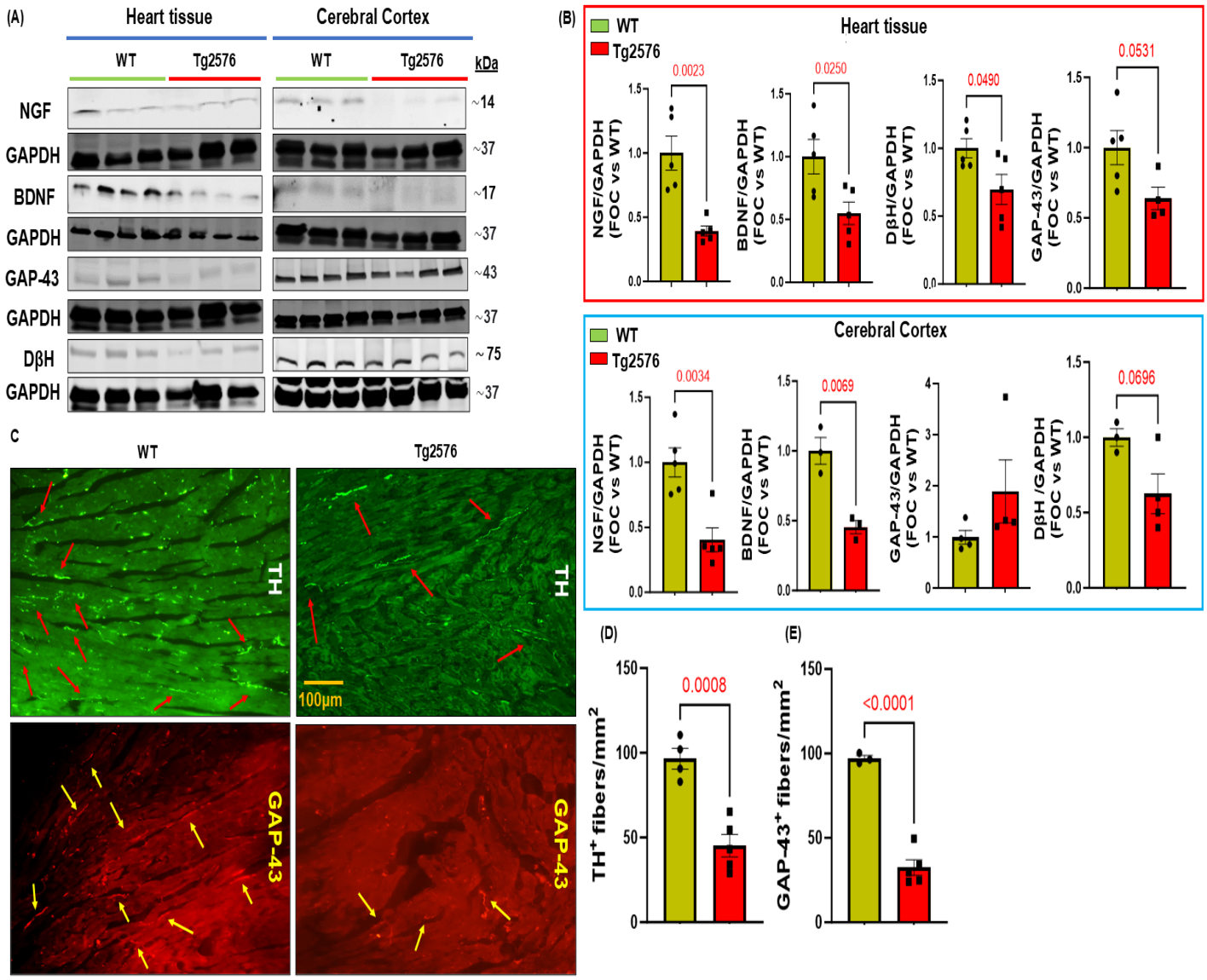

Figure 2. Alzheimer's disease pathology negatively impacts the neuro-signaling pathway in the brain/heart axis of Tg2576 mice. (**A-B**): Representative immunoblots (**A**) and densitometric analysis (**B**) showing levels of NGF, BDNF, GAP-43, and dβh in total heart tissue and cerebral cortex lysates from WT and Tg2576 mice. GAPDH levels were used as a loading control. (**C-E**): Digital images (**C**, scale bar 100μm) and quantifications (**D-E**) showing cardiac adrenergic nerve fibers, labeled with anti-tyrosine-hydroxylase (TH, in green) (**D**), and cardiac regenerating nerve endings, labeled with anti-neuronal regeneration marker (GAP-43, in red) (**E**), in cardiac sections from WT and Tg2576 mice. n=3-5 mice/group. Data are presented as a mean±SEM. *P<0.05 and vs WT. Student t-tests have been performed between the groups.

Figure 3

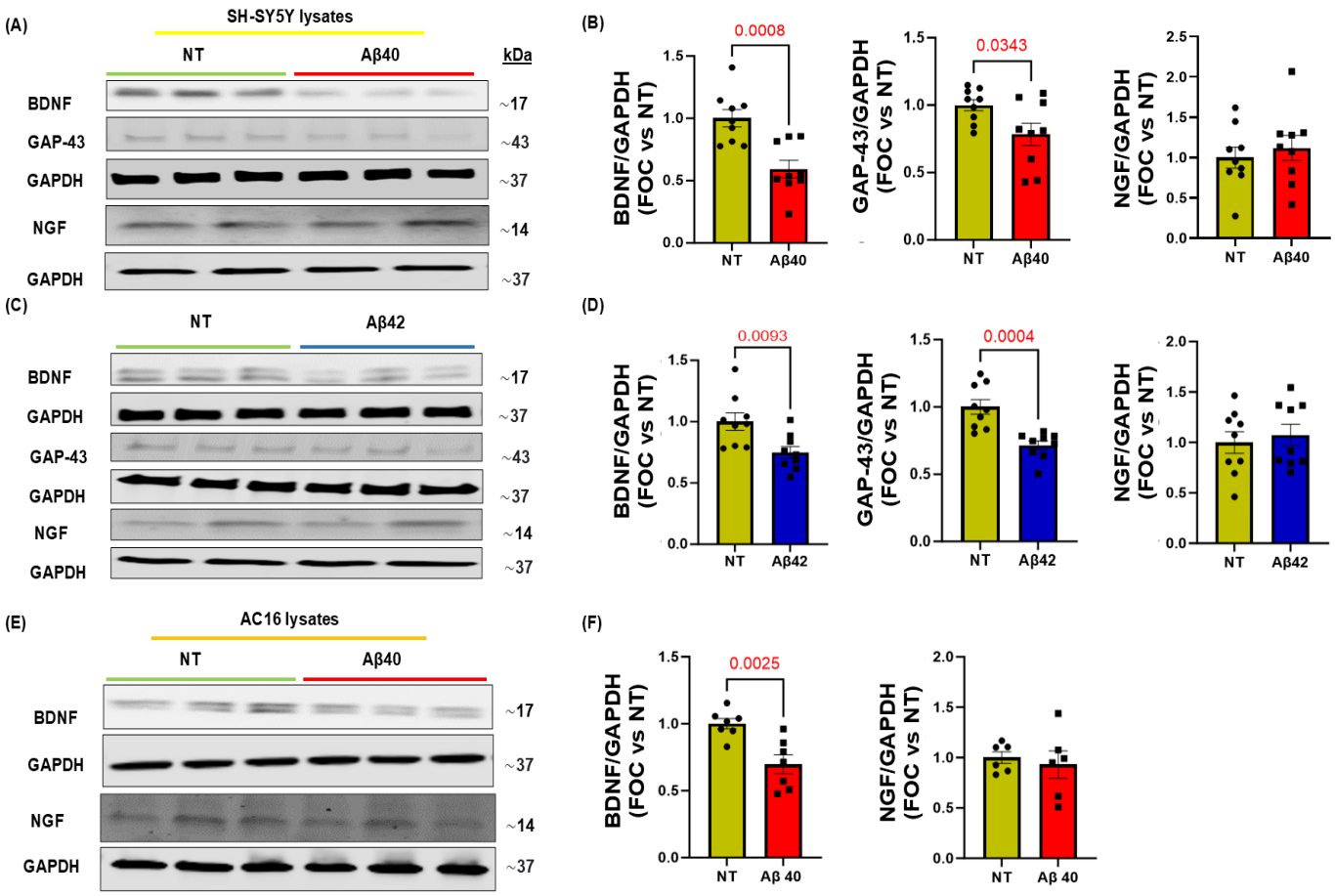

Figure 3. Effects of human Aβ40 or Aβ42 oligomers on neurotrophic factors in neuronal cells (SH-SY5Y) and human cardiomyocytes (AC16). (**A-D**): Representative immunoblots (**A-C**) and densitometric analysis (**B-D**) of multiple independent experiments to evaluate BDNF, NGF, and GAP-43 protein levels (**B-D**) in human neuroblastoma cells (SH-SY5Y) stimulated with human Aβ40 or Aβ42 oligomers for 16 h. GAPDH levels were used as a loading control. (**E-F**): Representative immunoblots (**E**) and densitometric quantitative analysis (**F**) showing protein levels of BDNF and NGF in total protein lysates from human cardiomyocytes (AC16) stimulated with human Aβ40 oligomers for 16 h. GAPDH levels were used as a loading control. n=6-9. Data are presented as a mean±SEM. *P<0.05 and vs NT. Student t-tests have been performed between the groups. (NT= Not Treated).

Figure 4

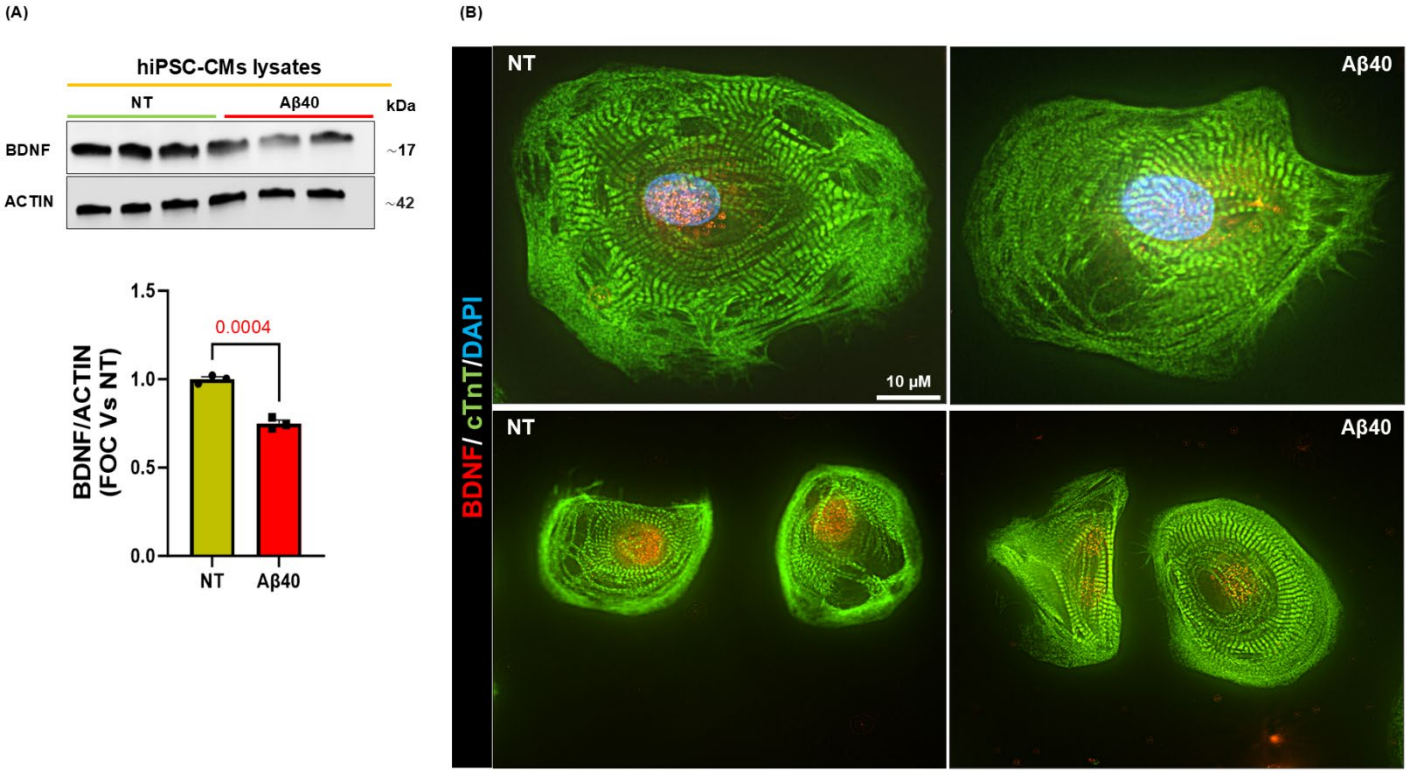

1058

1059 **Figure 4. Aβ40 oligomers induce BDNF downregulation in human-induced**
1060 **pluripotent stem cell-derived cardiomyocytes (hiPSC-CMs).** (**A**) Representative
1061 immunoblots (upper panels) and densitometric quantitative analysis (lower panel)
1062 showing protein levels of BDNF in total protein lysates from hiPSC-CMs stimulated
1063 with human Aβ40 oligomers for 20h. ACTIN levels were used as loading control. (**B**)
1064 Representative digital images (scale bar 10µm) of hiPSC-CMs stained with BDNF
1065 (red), cardiac Troponin T (cTnT, in green), and DAPI (blue). n=3. Data are presented
1066 as a mean±SEM. *P<0.05 and vs NT. Student t-tests have been performed between
1067 the groups. (NT= Not Treated).

1068

1069

1070

1071

1072

1073

Figure 5

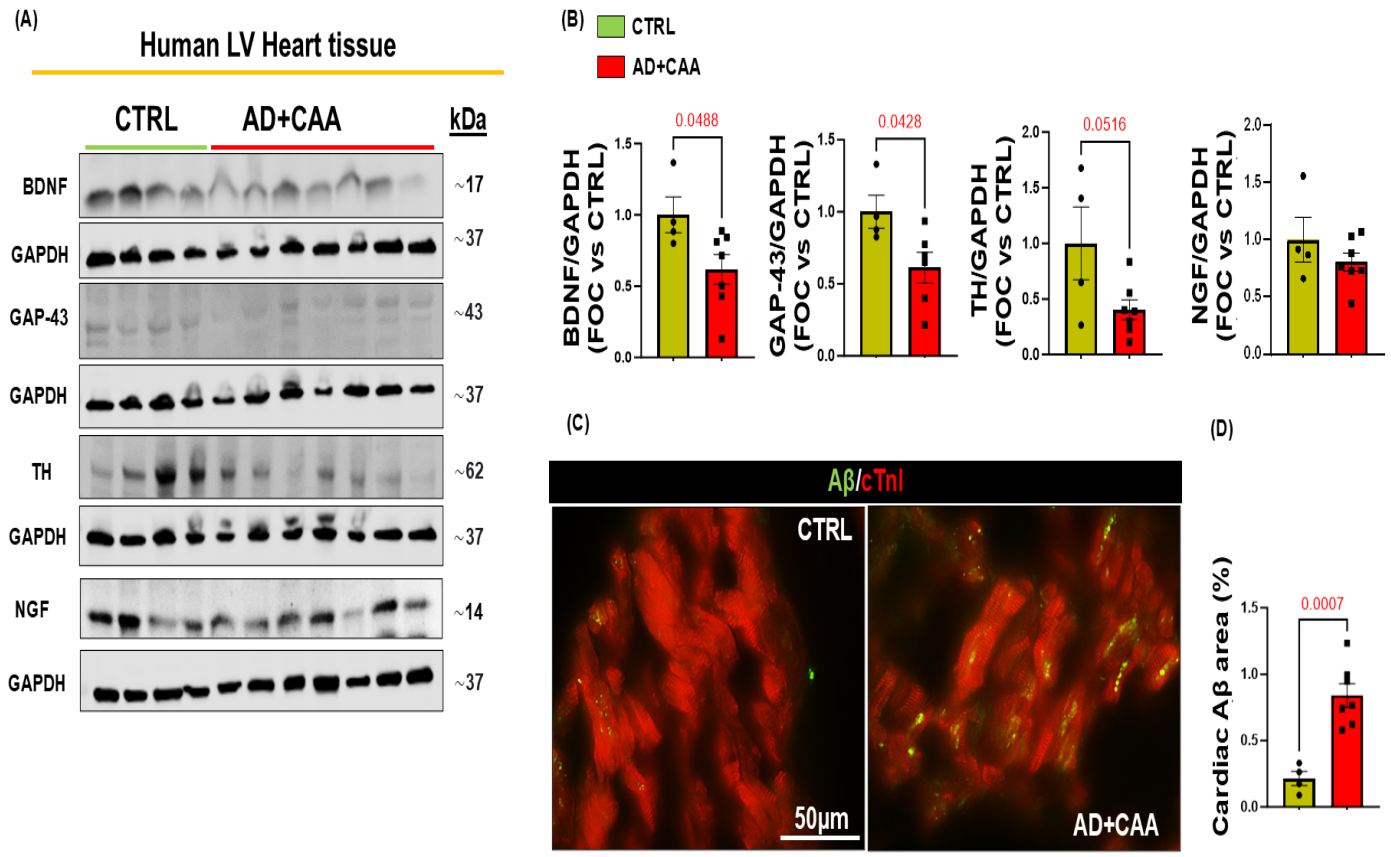

1074

1075 **Figure 5. Myocardial neuro-signaling impairment and Aβ deposits in human**
1076 **post-mortem cardiac tissue of AD subjects.** (**A-B**): Representative immunoblots
1077 (**A**) and densitometric analysis (**B**) showing reduced levels of BDNF, GAP-43, TH, but
1078 not NGF in total human LV lysates of patients with AD+CAA compared to healthy
1079 donors (CTRL). GAPDH levels were used as a loading control. (**C-D**): Representative
1080 digital images (**C**, scale bar 50µm), and quantification (**D**) of the LV sections from
1081 CTRL and AD+CAA subjects stained with Aβ aggregates (in green) and cardiac
1082 Troponin I (cTnI, in red). n=4-7 subjects/group. Data are presented as a mean±SEM.
1083 *P<0.05 and vs CTRL. Student t-tests have been performed between the groups.

1084

1085

1086

1087

Figure 6

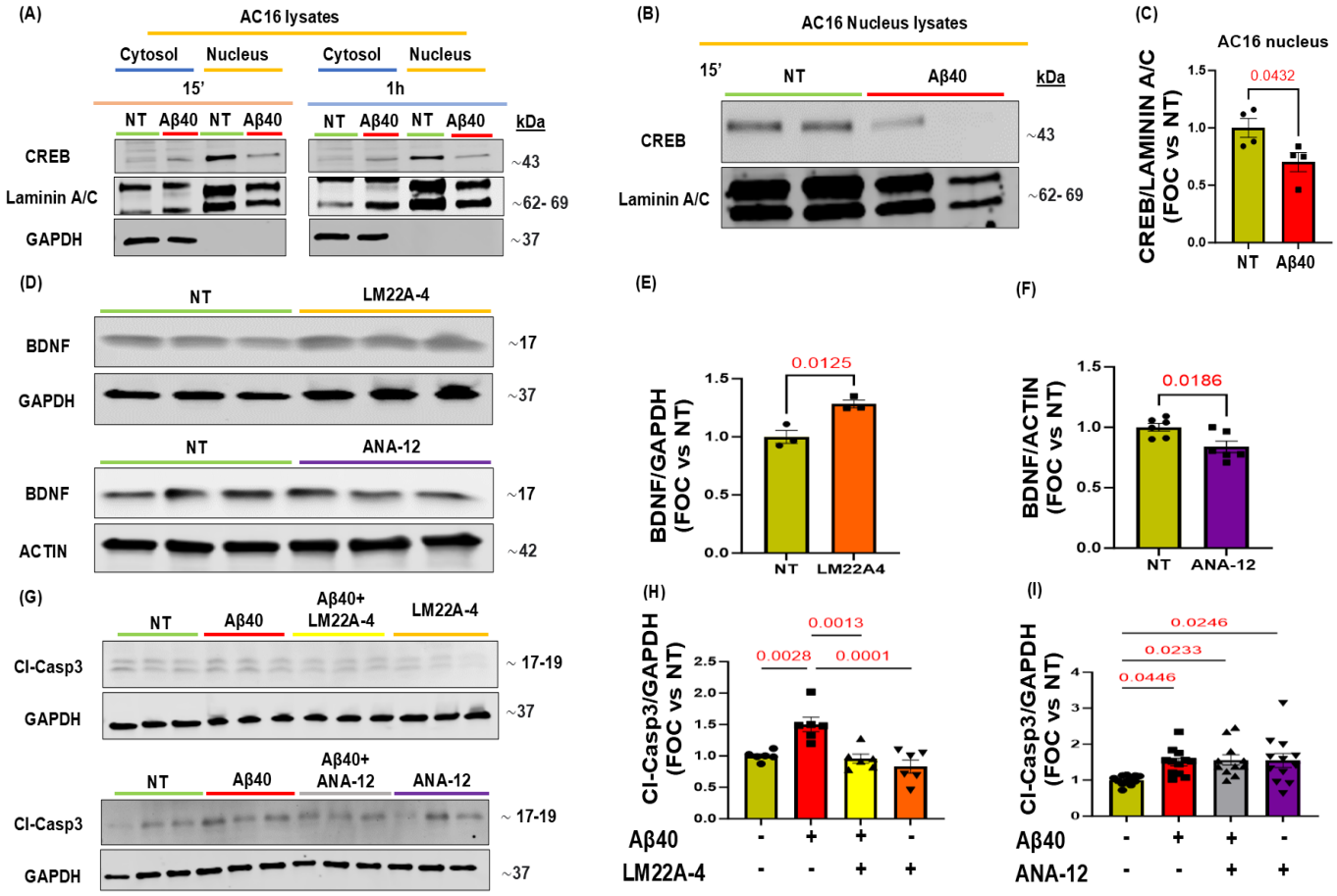

Figure 6. CREB signaling is impaired by Aβ40 oligomers and a TrkB agonist reduces Aβ40-mediated caspase 3 activation in human cardiomyocytes (AC16 cells). (**A-C**): Representative immunoblots (**A-B**) and densitometric quantitative analysis (**C**) of multiple independent experiments to evaluate CREB levels in nuclear extracts isolated from human cardiomyocytes (AC16) stimulated with human Aβ-40 oligomers for 15 minutes or 1h. LAMININ A/C levels were used as a nuclear loading control. (**D-F**): Representative immunoblots (**D**) and densitometric quantitative analysis (**E-F**) showing protein levels of BDNF in total protein lysates from human cardiomyocytes (AC16) stimulated with TrkB agonist LM22A-4 (100 nM) or TrkB antagonist ANA-12 (30 μM) for 16 h. GAPDH and ACTIN levels were used as loading controls. n=3-6. Data are presented as a mean±SEM. *P<0.05 and vs NT. Student t-tests have been performed between the groups. (**G-I**): Representative immunoblots (**G**) and densitometric quantitative analysis (**H-I**) of multiple independent experiments to evaluate Cleaved-Caspase 3 (Cl-Casp3) in AC16 cells stimulated with human Aβ-40 oligomers for 16 h. Before Aβ-40 oligomers treatment, cells were pretreated with

1104 either LM22A-4 (100 nM, top panel), or ANA-12 (30 μM, bottom panel) for 1 h. GAPDH
1105 levels were used as a loading control. n=6-12. One-way ANOVA with Tukey's multiple
1106 comparisons post hoc test: *P<0.05 and vs NT. (NT= Not Treated).

1107

Table 1

Demographic features of the individual cases from the clinical population.

Age	Ethnicity /Gender	Group	Associated Diseases and Comorbidities
53	CM	CTRL	Adenocarcinoma, Status post-Whipple procedure and liver transplantation, Hydroceles, Pulmonary vascular congestion, Hepatic congestion
75	CM	CTRL	Renal collecting duct carcinoma, Status post-Whipple procedure with gastric bypass and cholecystectomy, Mild cardiomegaly, Aorta Atherosclerosis, Testicular atrophy
81	CM	CTRL	Prostatic adenocarcinoma, Bilateral end-stage lung with honeycombing fibrosis (idiopathic pulmonary fibrosis with bronchiectasis by history), Cardiomegaly with left ventricular myocardial hypertrophy, Hepatomegaly, Hepatitis, Acute tubulointerstitial nephritis
90	CF	CTRL	Bilateral renal atrophy with mild nephrosclerosis and cortical cysts, Generalized atherosclerosis, Chronic esophagitis, Cardiomegaly with left ventricular myocardial hypertrophy, Hepatic centrilobular congestion, Chronic thyroiditis
74	CF	AD+CAA	Clear cell renal cell carcinoma, Cardiomegaly with left ventricular myocardial hypertrophy, Atherosclerosis, thoracic and abdominal aorta; Pulmonary vascular congestion; Hepatic atrophy; Status post thyroidectomy; Status post hysterectomy and bilateral salpingo-oophorectomy
85	CM	AD+CAA	History of prostatic carcinoma, status post prostatectomy, Aortic atherosclerosis, Left ventricular myocardial hypertrophy, Pulmonary fibrosis and bronchiolar metaplasia, Chronic esophagitis, Benign renal cysts, bilateral, Pancreatic and Testicular atrophy, Thyroid Nodular goiter, Status post cholecystectomy and Status post appendectomy
86	CF	AD+CAA	Acute bronchopneumonia, Mild cardiomegaly with left ventricular myocardial hypertrophy, Aortic atherosclerosis, Benign endometrial polyp, Nodular goiter, Osteopenia, Hepatic chronic passive congestion, Enchondroma, lumbar vertebra, Renal cortical cysts, History of plasmacytoma
87	CM	AD+CAA	Acute bronchopneumonia; Pulmonary interstitial fibrosis, Cardiomegaly with left ventricular myocardial hypertrophy, Aortic atherosclerosis, Chronic pyelonephritis, Bilateral renal atrophy, Hepatic atrophy, Cholelithiasis, Parathyroid adenoma, S/P radical prostatectomy, history of prostate cancer, S/P cardiac pacemaker placement
87	CM	AD+CAA	Acute bronchopneumonia, Aortic atherosclerosis, Hepatic chronic passive congestion, Prostatic glandular hyperplasia, Testicular atrophy, Mild chronic thyroiditis, Status post cardiac pacemaker, Diverticulosis, Benign renal cortical cyst, right
89	CF	AD+CAA	Acute bronchopneumonia, Calcified granuloma, Aortic atherosclerosis, Pleural fibrotic plaque, Mild calcification, aortic valve, Atherosclerotic stenosis, Cardiomegaly, Hepatic atrophy, Mild chronic lymphocytic thyroiditis, Status post hysterectomy and bilateral salpingo-oophorectomy
90	CF	AD+CAA	Pancreatic ductal adenocarcinoma, Cardiomegaly, Atherosclerosis, thoracic and abdominal aorta, Emphysema, Diverticulosis, Hashimoto's thyroiditis, Status post supracervical hysterectomy, Benign atrophic and fibrotic breast tissue, Osteopenia

1108

1109 **Table 1. Anatomopathological and demographic characteristics of the selected**
1110 **clinical cohort.** *P values of the patients age = 0.1253 vs CTRL. Student t-tests have
1111 been performed between the groups. **Abbreviations**: **CF**= Caucasian Female, **CM**=
1112 Caucasian Male, **Ctrl**= Control, **AD**= Alzheimer's Disease, **CAA**= Cerebral Amyloid
1113 Angiopathy.

1114

1115

1116

1117

Supplemental Table 1

Echocardiographic analysis	13 months old	
Parameters	**WT**	**Tg2576**
Heart rate (bpm)	446.75±26.25	444.44±32.49
LVEDD (mm)	3.99±0.39	4.54±0.33
LVESD (mm)	2.54±0.21	3.47±0.33**
LVEDV (µl)	71.62±14.59	95.44±16.43
LVESV (µl)	24.13±4.40	50.58±12.00**
EF (%)	66.34±2.68	47.24±5.60***
FS (%)	36.23±2.18	23,70±3.38***
LVAW;d (mm)	0.86±0.10	0.98±0.25
LVAW;s (mm)	1.21±0.21	1,37±0,35
LVPW;d (mm)	1.11±0.15	0.72±0.14**
LVPW;s (mm)	1.53±0.18	1.00±0.12**
LV Mass AW (mg)	155.33±26.40	159.41±37.63
Cardiac output (ml/min)	14.42±1.28	14.75±2.81

Supplemental Table 1. Echocardiographic evaluation. Conventional echocardiographic parameters were measured in 13-month-old WT and Tg2576 mice: heart rate, left ventricular (LV) end diastolic diameter (LVEDD), end systolic diameter (LVESD), end-diastolic volume (LVEDV), end systolic volume (LVESV), ejection fraction (EF), fractional shortening (FS), anterior wall in diastole (LVAW;d) and systole (LVAW;s), posterior wall in diastole (LVPW;d) and systole (LVPW;s), mass of the anterior wall (LV Mass AW), and cardiac output. n=4-6 mice/group. Data are presented as a mean±SEM. *P<0.05, **p<0.01, and ***p<0.001 vs WT. Student t-tests were performed between the groups.

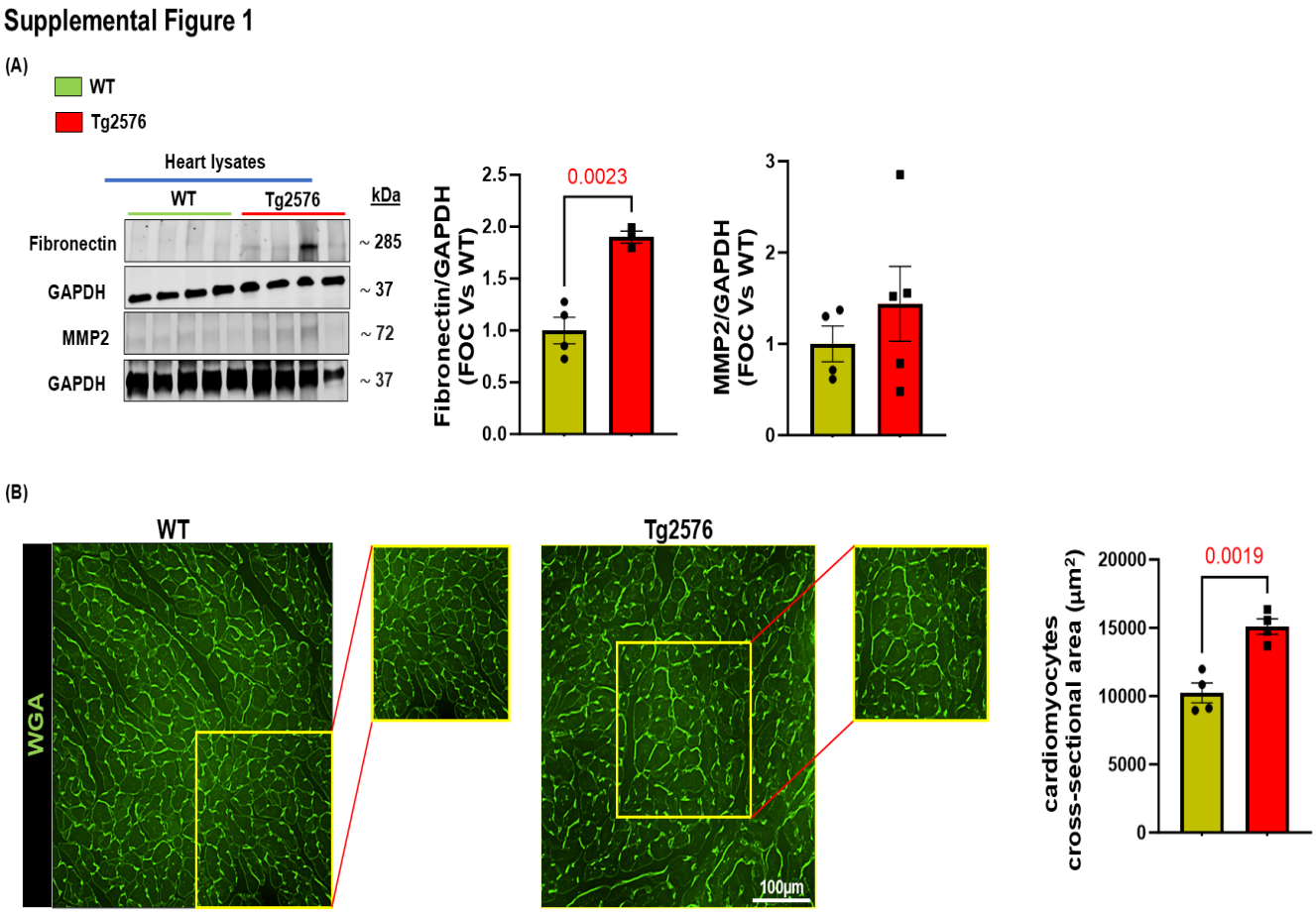

Supplemental Figure 1. Cardiac adverse remodeling in 13-month-old Tg2576-AD mouse heart. (**A**) Representative immunoblots (left panels) and densitometric quantitative analysis (right panels) showing protein levels of fibronectin and MMP2 in total cardiac lysates from WT and Tg2576 mice. GAPDH levels were used as a loading control. (**B**) Representative digital images (left panels, scale bar 100µm), and quantification (right panel) of the cardiomyocyte cross-sectional area (CSA) in cardiac sections from WT and Tg2576 mice stained with WGA. n=4-5 mice/group. Data are presented as a mean±SEM. *P<0.05 and vs WT. Student t-tests have been performed between the groups.

Supplemental Figure 2

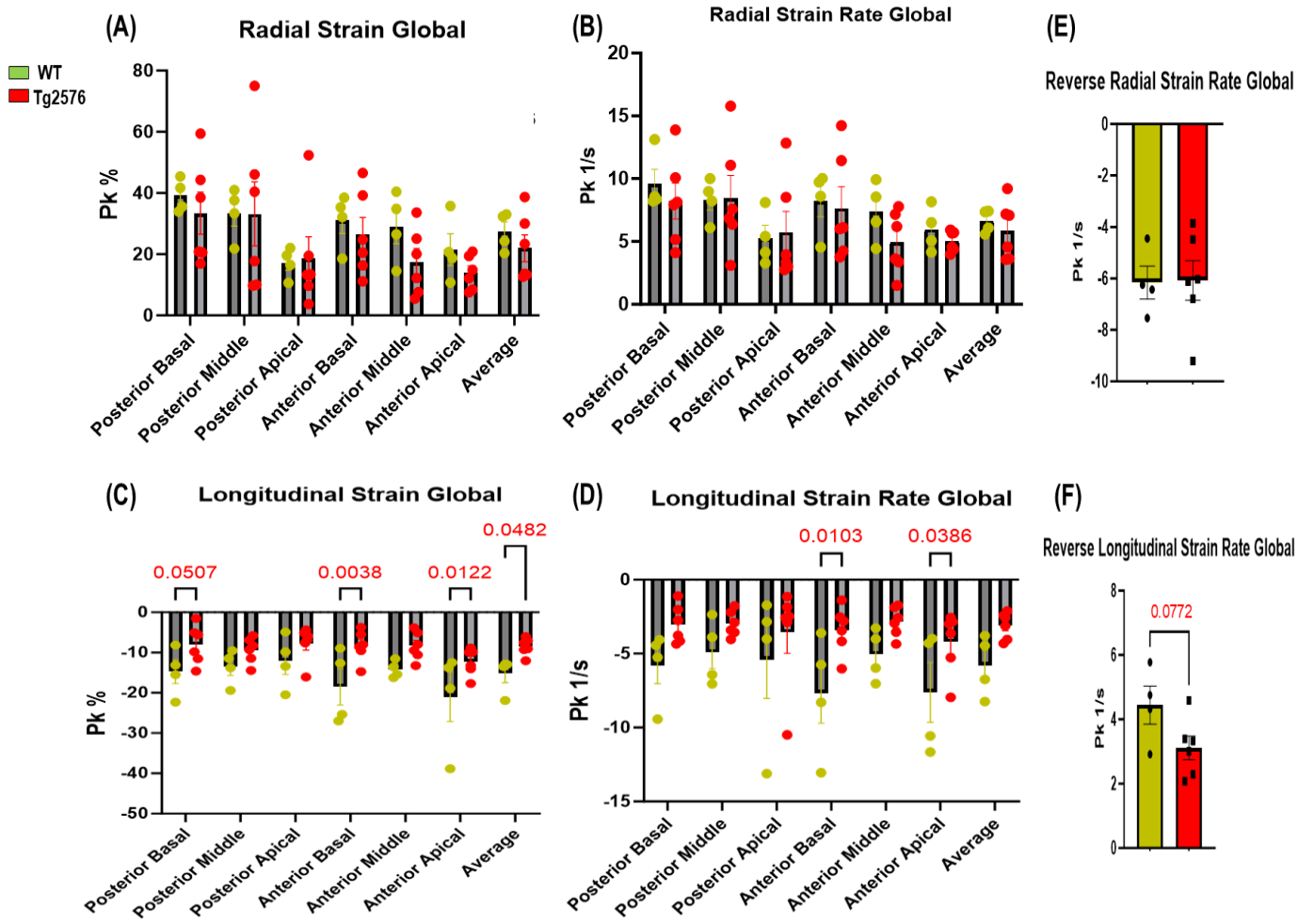

Supplemental Figure 2. Longitudinal strain and strain rate LV contractility are impaired in Tg2576 AD mice. Radial and longitudinal strain or strain rate measured at six LV segments as well as their average (**A-D**), and reverse (diastolic) radial (**E**) and longitudinal (**F**) SR global in 13 months old WT and Tg2576 mice were evaluated using speckle-tracking-based strain echocardiography. Data are presented as a mean±SEM. *P<0.05 and vs WT. n=4-6 mice/group. Two-way ANOVA with Tukey's multiple comparisons post hoc test (**A-D**), and student t-tests (**E-F**) have been performed between the groups.

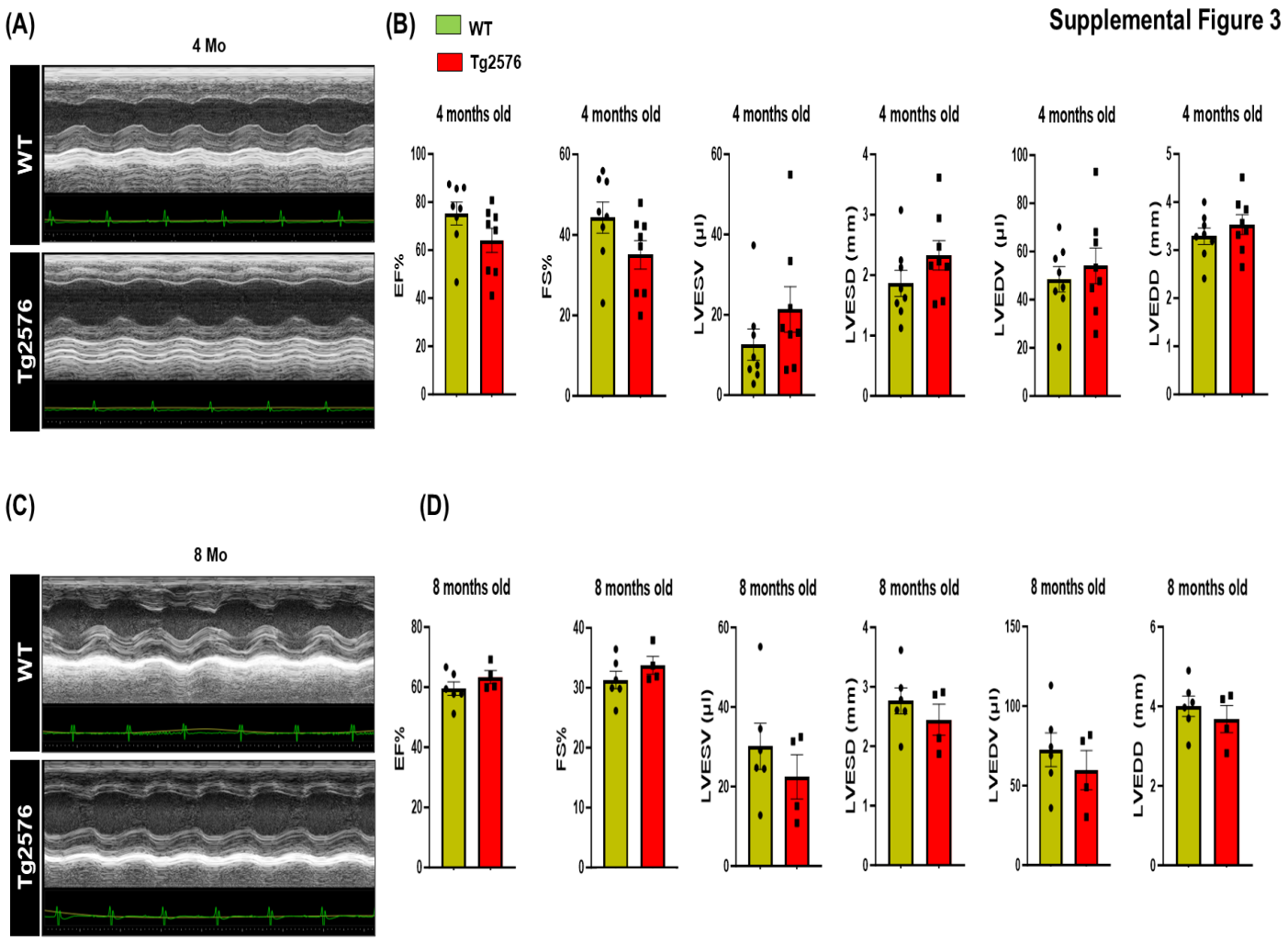

Supplemental Figure 3. Cardiac function is not affected in 4 or 8 months old Tg2576 mice. (**A-C**) Representative M-mode echocardiography images of WT and Tg2576 mice show no difference between the experimental groups. (**B-D**) Ejection fraction (EF%) and fractional shortening (FS%) percentage, left ventricular end-systolic and diastolic diameters (LVESD, LVEDD), and left ventricular end-systolic and diastolic volumes (LVESV, LVEDV) of age-matched (4 and 8-month-old) Tg2576 mice and WT littermates. n=4- 8 mice/group. Data are presented as a mean±SEM. *P<0.05 and vs WT. Student t-tests have been performed between the groups.

Supplemental Figure 4

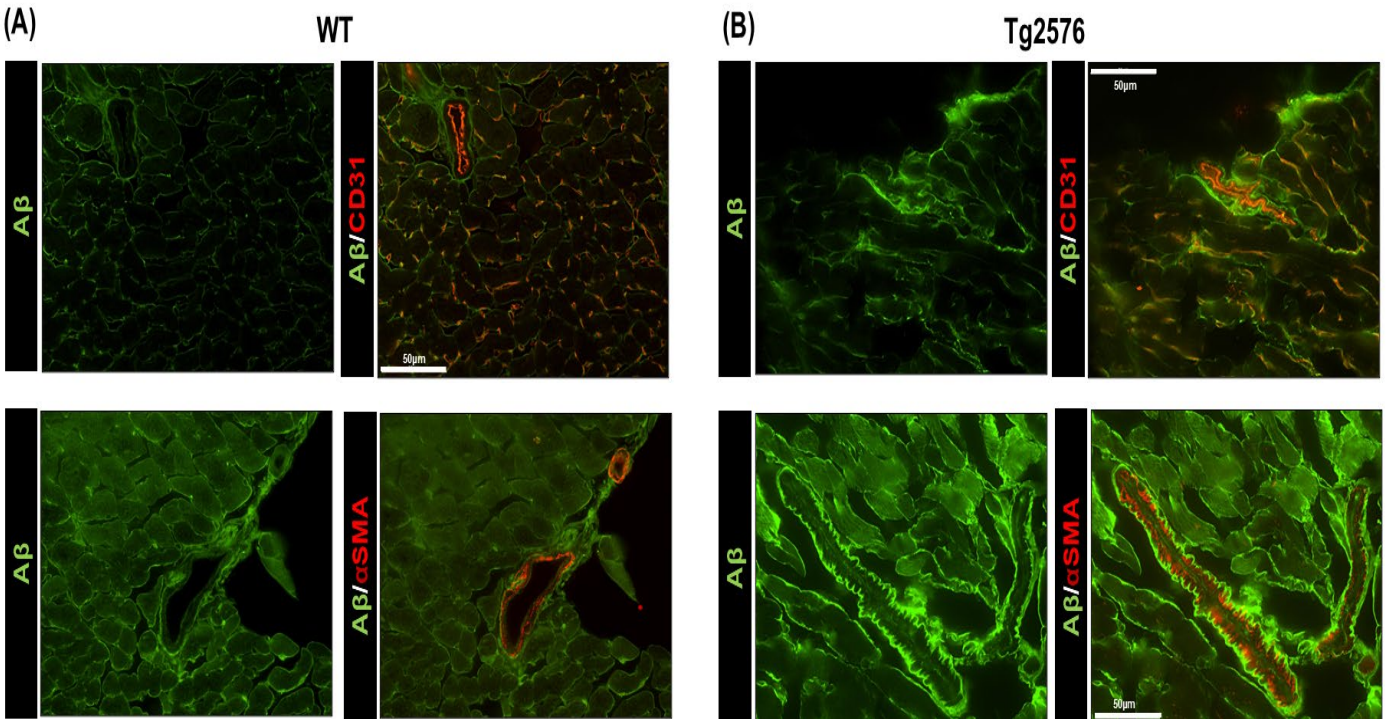

Supplemental Figure 4. Amyloid-β surrounds cardiac vessels and infiltrates the vascular basal lamina. (**A**-**B**) Representative digital images (upper panels, scale bar 50μm) showing vessels (endothelial cells stained with CD31, in red) and Aβ (in green), and representative digital images (lower panels; scale bar 50μm) showing α-smooth muscle actin (αSMA, staining vascular smooth muscle cells, in red) and Aβ (in green) in cardiac sections from 13 months old WT and Tg2576 mice.

Supplemental Figure 5

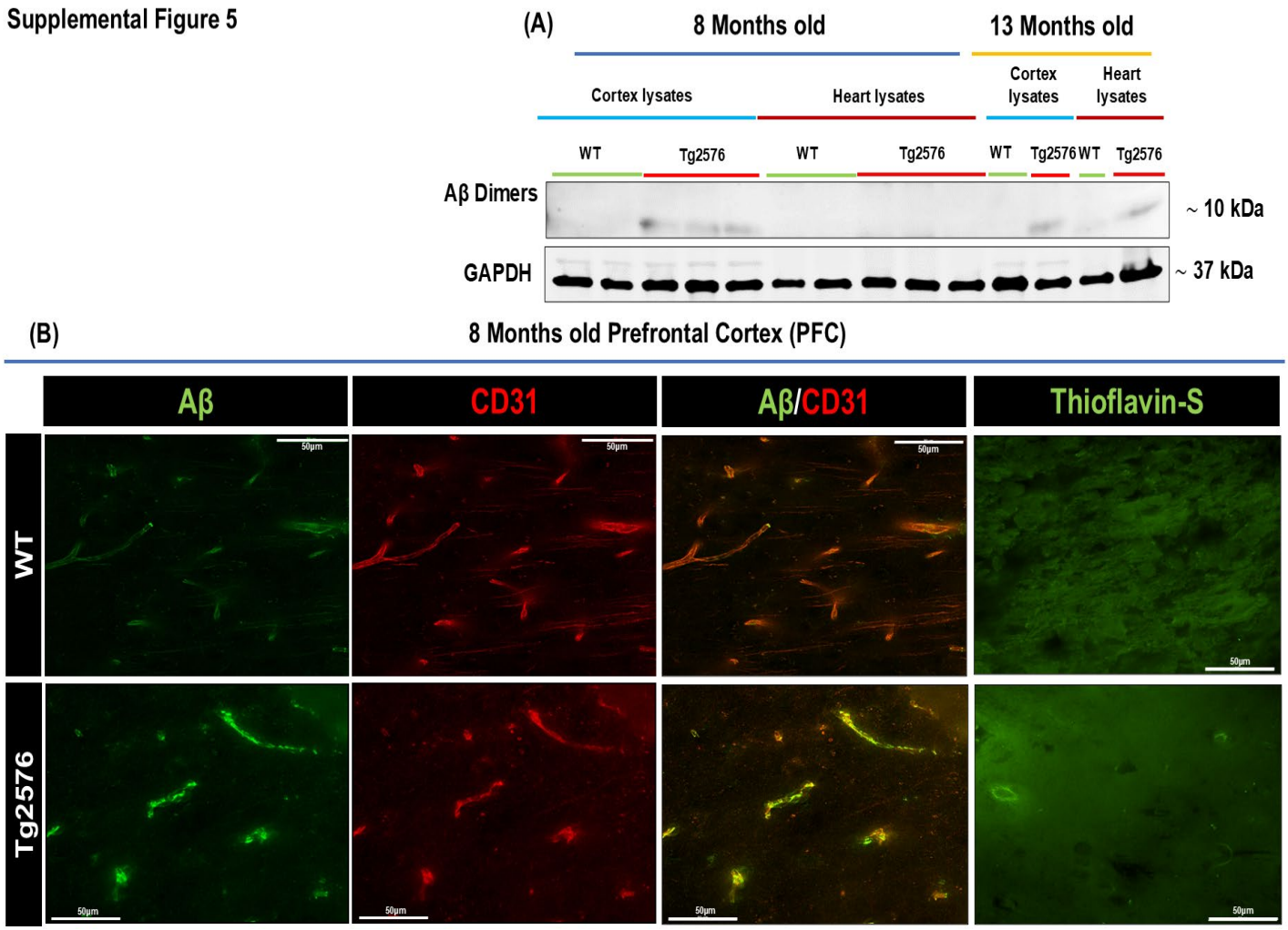

Supplemental Figure 5. Amyloid-β deposits in vessels of 8 months-old Tg2576 prefrontal cortex (PFC), but not in heart tissue. (**A**) Representative immunoblots show Aβ dimers in total cardiac lysates from WT and Tg2576 mice. Tg2576 cerebral cortex lysate was used as an internal positive control. GAPDH levels were used as a loading control. (**B**) Representative digital images (scale bar 50μm) showing vessels (stained with CD31, in red) and Aβ deposits (in green). Right panels: representative digital images (right panels; scale bar 50μm) showing β- sheet conformation (fibrillar) amyloid marked with Thioflavin-S (in green) in the prefrontal cortex (PFC), in 8-months old WT and Tg2576 mice.

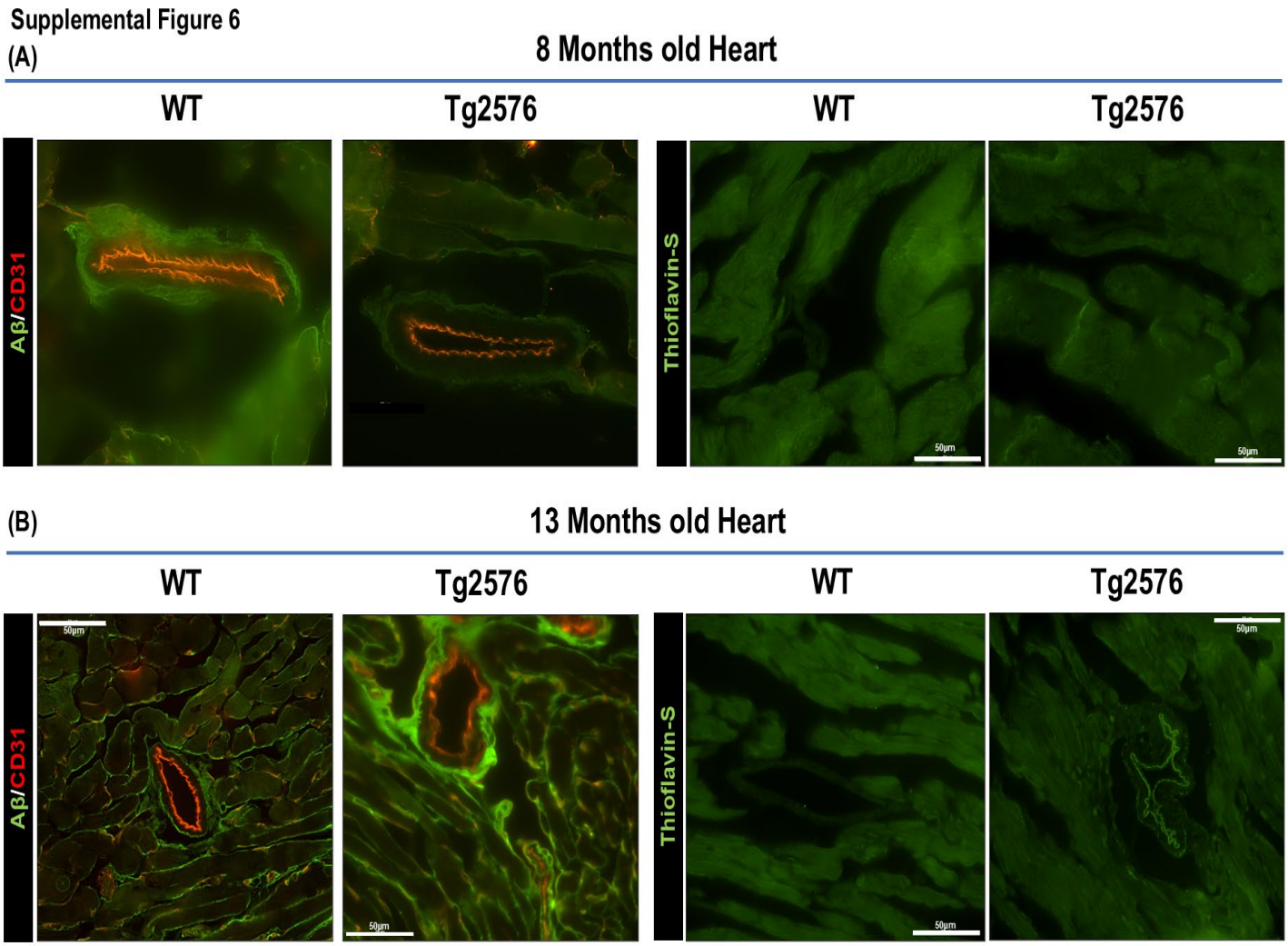

Supplemental Figure 6. AD pathology affects the cardiac vascular network in 13-month-old Tg2576 mice. (**A-B**) Representative digital images (left panels, scale bar 50μm) showing vessels (stained with CD31, in red) and Aβ deposits (in green), and representative digital images (right panels; scale bar 50μm) showing β-sheet conformation of amyloid marked with Thioflavin-S (in green) in cardiac sections from WT and Tg2576 mice.

Supplemental Figure 7

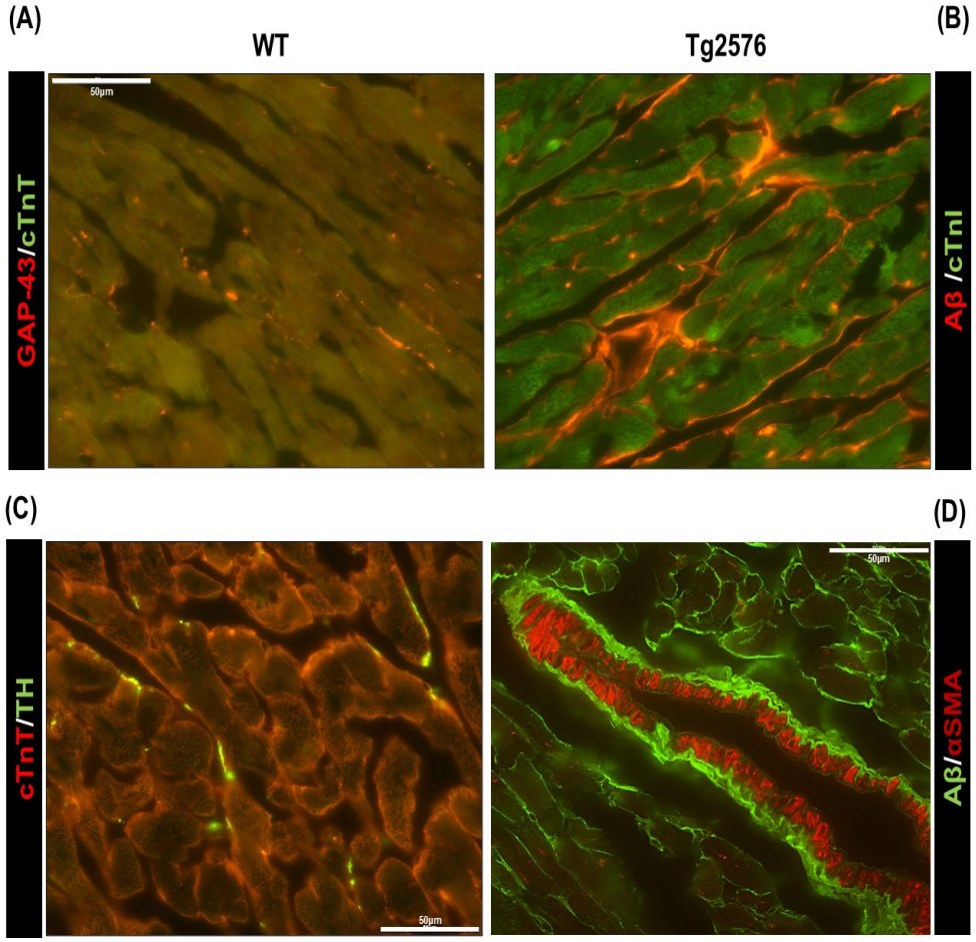

1211

1212 **Supplemental Figure 7.** Representative digital images (scale bar 50μm) of cardiac
1213 sections from 13-month-old WT and Tg2576 mice stained with (**A**) anti-neuronal
1214 regeneration marker (GAP-43, in red) and cardiac Troponin T (cTnT, in green). (**B**) Aβ
1215 (in red) and cardiac Troponin I (cTnI, in green). (**C**) anti-tyrosine-hydroxylase (TH, in
1216 green) and cardiac Troponin T (cTnT, in red). (**D**) Aβ (in green) and α-smooth muscle
1217 actin (α-SMA, in red).

1218

1219

1220

1221

1222

1223

Supplemental Figure 8

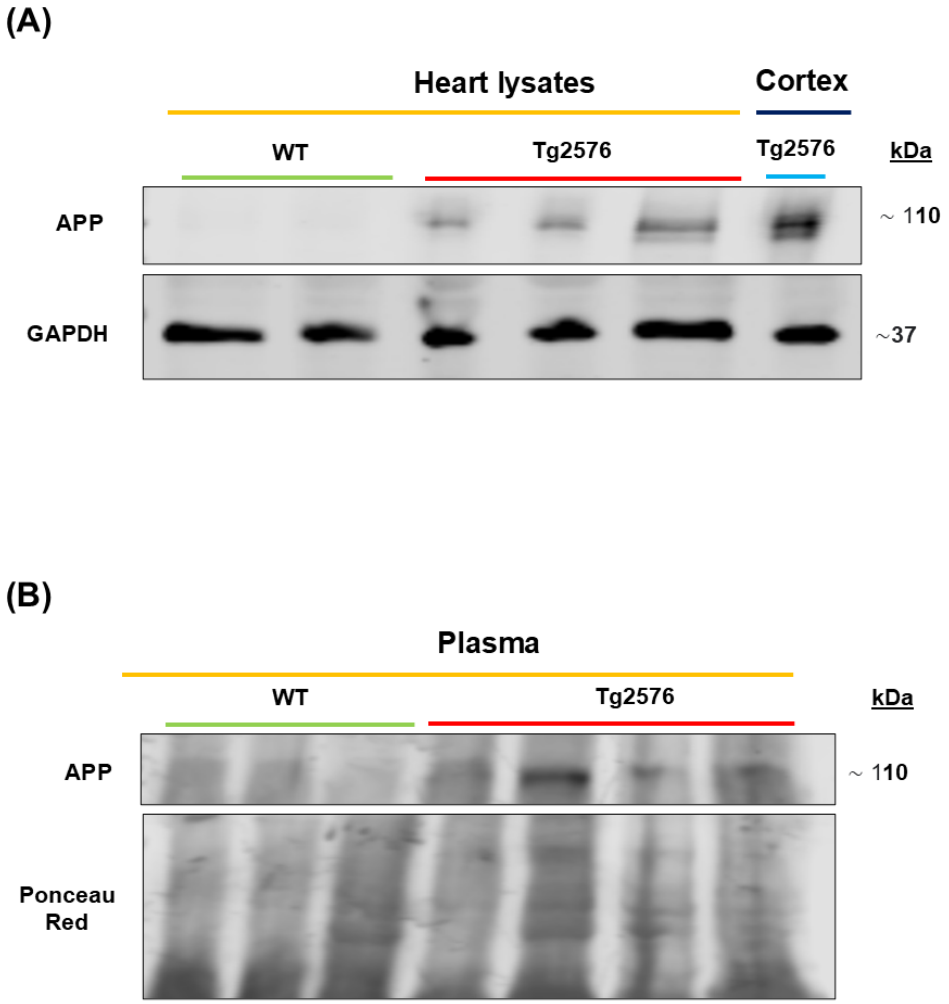

1224

1225 **Supplemental Figure 8. The Amyloid precursor protein (APP) is present in**
1226 **plasma and heart tissue of the 13-month-old Tg2576-AD model.** (**A-B**)
1227 Representative immunoblots showing protein levels of APP in total cardiac lysates
1228 (upper panel) and plasma APP levels (lower panel) in 13-month-old WT and Tg2576
1229 mice. Tg2576 cortex lysate was used as an internal positive control. GAPDH levels or
1230 ponceau red were used as respective loading controls.

1231

1232

1233

1234

1235

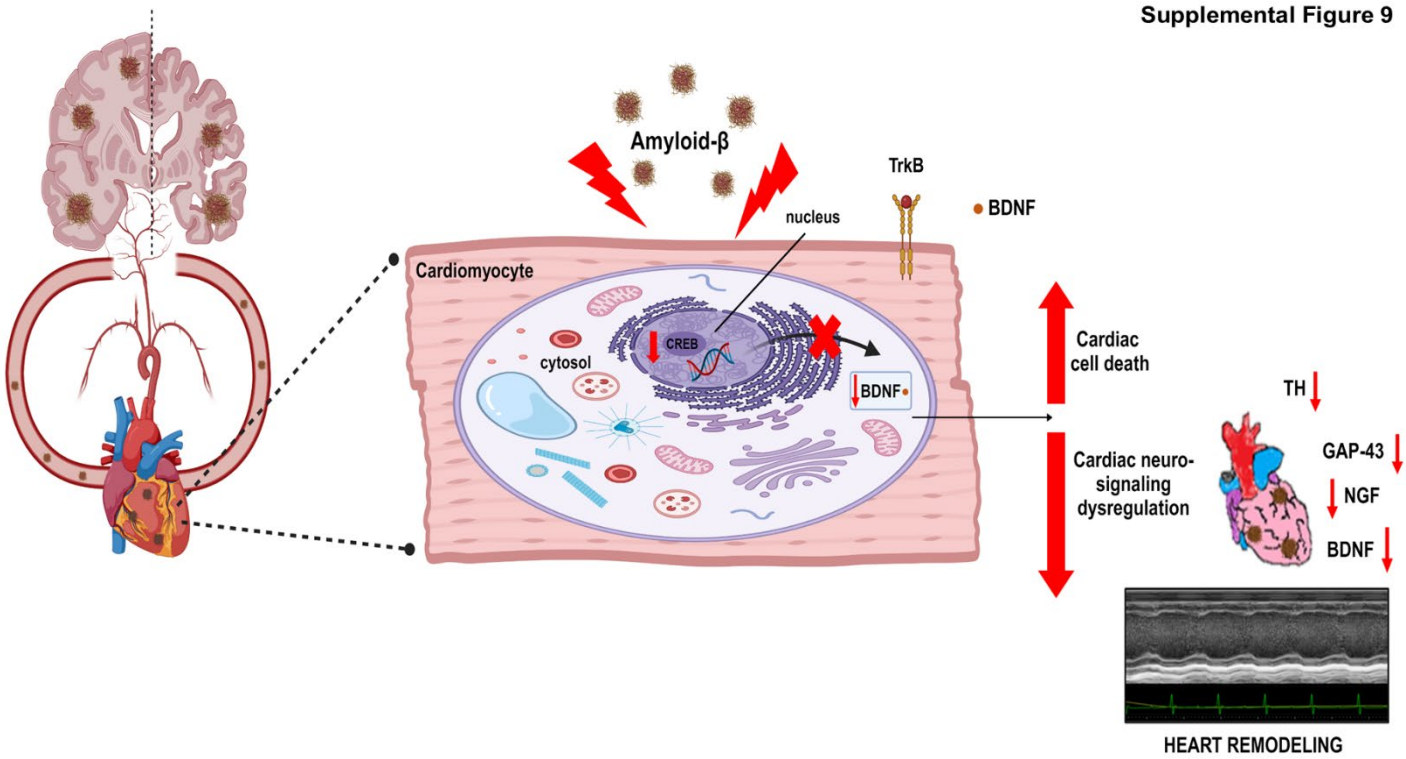

1236

1237 **Supplemental Figure 9. Conceptual scheme of the study**. Amyloid- β aggregates,
1238 present in the heart parenchyma of AD mouse models and AD human hearts, induce
1239 adverse cardiac remodeling and myocardial denervation through cardiac
1240 TrkB/CREB/BDNF neurotrophic signaling axis dysregulation, ultimately resulting in
1241 impaired cardiac physiology.

1242

1243